1

2

3

4

Human gut microbiota interactions shape the long-term growth dynamics and evolutionary adaptations of *Clostridioides difficile*

7

8 Jordy Evan Sulaiman [1], Jaron Thompson [2], Pak Lun Kevin Cheung [1], Yili Qian [1], Jericha

9 Mill [1], Isabella James [5], Eugenio I. Vivas [3, 6], Judith Simcox [7] and Ophelia Venturelli [1, 2,

10 3, 4, *]

11

12 [1] Department of Biochemistry, University of Wisconsin-Madison, Madison, WI, USA.

13 [2] Department of Chemical & Biological Engineering, University of Wisconsin-Madison,

14 Madison, WI, USA.

15 [3] Department of Bacteriology, University of Wisconsin-Madison, Madison, WI, USA.

16 [4] Department of Biomedical Engineering, University of Wisconsin-Madison, Madison,

17 WI, USA.

18 [5] Integrated Program in Biochemistry, University of Wisconsin-Madison, Madison, WI,

19 USA.

20 [6] Gnotobiotic Animal Core Facility, University of Wisconsin-Madison, Madison, WI, USA.

21 [7] Howard Hughes Medical Institute, Department of Biochemistry, University of

22 Wisconsin-Madison, Madison, WI, USA.

23

24 * To whom correspondence should be addressed: venturelli@wisc.edu

ABSTRACT

Clostridioides difficile can transiently or persistently colonize the human gut, posing a risk factor for infections. This colonization is influenced by complex molecular and ecological interactions with human gut microbiota. By investigating *C. difficile* dynamics in human gut communities over hundreds of generations, we show patterns of stable coexistence, instability, or competitive exclusion. Lowering carbohydrate concentration shifted a community containing *C. difficile* and the prevalent human gut symbiont *Phocaeicola vulgatus* from competitive exclusion to coexistence, facilitated by increased cross-feeding. In this environment, *C. difficile* adapted via single-point mutations in key metabolic genes, altering its metabolic niche from proline to glucose utilization. These metabolic changes substantially impacted inter-species interactions and reduced disease severity in the mammalian gut. In sum, human gut microbiota interactions are crucial in shaping the long-term growth dynamics and evolutionary adaptations of *C. difficile*, offering key insights for developing anti-*C. difficile* strategies.

INTRODUCTION

Clostridioides difficile is an opportunistic intestinal pathogen that can cause severe damage to the colon. Antibiotic treatment is highly associated with *C. difficile* infection (CDI), highlighting that microbial ecology of the human gut microbiome disrupted by antibiotics is a major determinant of *C. difficile's* ability to colonize and induce infections [1]. *C. difficile* has been observed in up to 17% of healthy human adults [2-6] and up to 20-40% of hospitalized patients [7-9], and it can colonize individuals for 12 months or longer [6,10,11]. Further, diarrheal events increase susceptibility to *C. difficile* and trigger long-term *C. difficile* colonization with recurrent blooms at yearlong time scales [12]. While human gut microbiota inter-species interactions with *C. difficile* have been identified over short timescales (~5 to 10 generations) [13,14], it is unclear how interactions shape the long-term growth dynamics and potential evolutionary adaptations of *C. difficile*. A deeper understanding of the ecological and molecular mechanisms shaping *C. difficile* growth over long timescales (hundreds of generations) could provide insights into mechanisms that inhibit or promote persistent colonization.

Although the impact of *C. difficile* colonization on the propensity for acquiring CDI remains unresolved [12,15], individuals harboring toxigenic *C. difficile* strains had a higher risk for the development of infection compared to non-colonized patients [16,17]. The incidence of community-acquired CDI is increasing [18]. Individuals harboring *C. difficile* could transmit it to others, serving as a reservoir for *C. difficile* [8,19-21]. By contrast, persistent colonization of non-toxigenic strains may reduce the chance of colonization with toxigenic strains due to competition and/or stimulating a protective immune response to *C. difficile* [22-28]. Colonization for extended periods of time can also shape *C. difficile* evolutionary adaptations [29-31]. For example, *C. difficile* acquired a mutation in the *treR* gene that confers enhanced sensitivity to trehalose, potentially due to increased consumption of trehalose in human diets [32]. This metabolic alteration was associated with

66 *C. difficile*'s hypervirulence [29], suggesting that key evolutionary adaptations can have a
67 major impact on pathogenic potential.

68   Community-level interactions have been shown to shape evolutionary adaptations
69 [33-35] and lead to distinct evolutionary trajectories compared to those observed in isolation.
70 Long-term culturing of communities constructed from the bottom up can reveal the effects
71 of community context on the mechanisms of adaptation [33,35-39]. This approach has been
72 used to study model organisms [33] or self-assembled communities from the soil
73 environment [36-42]. For example, constituent community members evolved to use waste
74 products generated by other species [36,43,44] and shift the community from strong
75 competition to coexistence [38]. Further, coevolution within a community promotes
76 ecological diversity and stability [39]. Increasing resource competition [45] or community
77 diversity [46] has been shown to slow the rate of evolutionary adaptation. By contrast,
78 positive interactions through cross-feeding promote evolutionary adaptation [34,47,48].
79 Organisms that interact via metabolite exchange evolved to enhance the production of
80 the exchanged metabolites to promote community fitness [34]. Finally, there are many
81 examples of species evolving new community interactions that were frequently positive
82 [38,47,49,50].

83   By building communities from the bottom up, we investigate the dynamics of *C.
84 difficile* in various human gut communities and different environmental contexts for
85 hundreds of generations. We demonstrate that *Eggerthella lenta* promotes stable
86 coexistence of *C. difficile* via a growth-promoting interaction. By contrast, *P. vulgatus* or
87 *Desulfovibrio piger* promotes instability in community dynamics across different nutrient
88 environments. Reducing the concentration of carbohydrates in the media shifts *C. difficile*
89 and *P. vulgatus* from competitive exclusion to coexistence by promoting metabolite
90 exchange. In this environment, *C. difficile* adapts via point mutations in key metabolic
91 genes. These mutations shift *C. difficile* metabolism from proline to glucose utilization,
92 substantially alter gut microbiota inter-species interactions, and reduce disease severity
93 in the murine gut. Further, we show that variation in nutrient landscape impacts the extent
94 of variability of *C. difficile* growth in human gut communities. *C. difficile* abundance is
95 lowered in an environment with a single highly accessible resource yet also displays
96 higher variability in growth over 261 generations compared to an environment with
97 multiple preferred carbohydrates. Overall, our study demonstrates how gut microbiota
98 inter-species interactions influence the long-term growth dynamics and evolutionary
99 adaptations of *C. difficile*, offering new insights for developing targeted treatments to
100 inhibit *C. difficile*.

RESULTS

Human gut species differentially impact C. difficile long-term growth in communities

C. difficile can colonize individuals at different stages of life for variable periods of time and the factors that determine these dynamics are largely unknown. Since gut microbial ecology is a major determinant of *C. difficile* colonization, we used bottom-up microbial community experiments to investigate how interactions shape the long-term growth dynamics of *C. difficile*. To this end, we cultured *C. difficile* DSM 27147 (R20291 reference strain of the epidemic ribotype 027) with 9 diverse human gut species in a defined media (DM) that supports their growth (**Fig. 1a, S1a, Table S1-2**) [51,52]. These human gut species are highly prevalent across individuals and span the phylogenetic diversity of the human gut microbiome [53]. The community features *Clostridium scindens* (CS), a species previously shown to inhibit the growth of *C. difficile* in gnotobiotic mice [54], *Clostridium hiranonis* (CH), which can inhibit *C. difficile* via metabolic niche overlap and lead to large shifts in *C. difficile* metabolism [55], and *Bacteroides* species (*Bacteroides uniformis* (BU), *Bacteroides thetaoitaomicron* (BT), *P. vulgatus* (PV)), which can inhibit or promote *C. difficile* growth in different environments [56-59]. Interactions between *D. piger* (DP), *E. lenta* (EL), *Collinsella aerofaciens* (CA), and *Prevotella copri* (PC) with *C. difficile* have also been extensively characterized on short timescales (~5-10 generations) [14,55]. We assembled all possible pairwise (9 total) and three-member communities (36 total) containing *C. difficile* and gut bacteria. The communities were cultured for 24 h, and an aliquot was transferred to fresh media with 40X dilution for 35 passages (~186 generations). We performed 16S rRNA sequencing to determine the relative abundance of each species and multiplied the relative abundance by the total biomass at each time point to estimate the absolute abundance of each species [14,60]. In addition, each species was individually cultured over time mirroring the same experimental design (**Fig. S1b**).
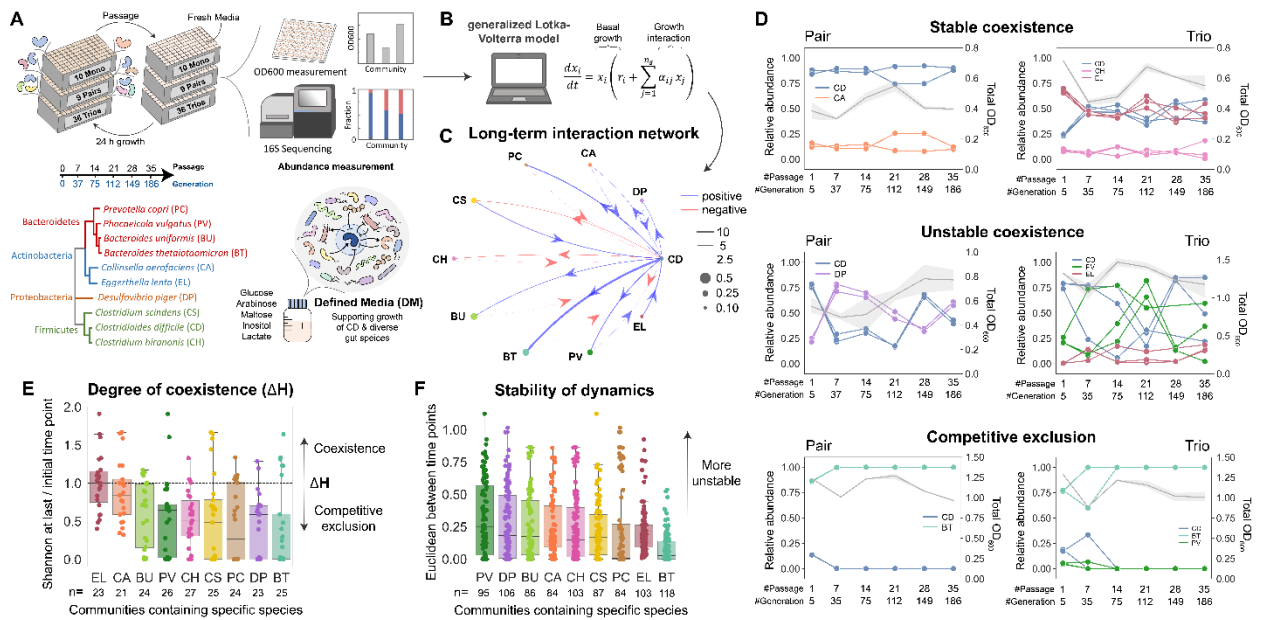
Figure 1. Long-term growth dynamics between *C. difficile* and human gut bacteria in pairwise and three-member communities. a, Schematic of the long-term growth experiment of *C. difficile* in human gut communities over 35 passages grown in the Defined Media (DM). The phylogenetic tree was generated from the 16S rRNA sequence of each species. Over time, aliquots of the cultures were subjected to OD_{600} measurement and multiplexed 16S rRNA sequencing to determine species abundances. **b**, Absolute abundance data from the long-term growth experiment are used to infer the parameters of a generalized Lotka–Volterra (gLV) model and elucidate the long-term interaction network of the communities (See **Methods, Table S3** DATASET001). **c**, Inferred long-term inter-species interaction network of the 9 gut species and *C. difficile* using growth data over 35 passages. Node size represents species carrying capacity and edge width represents the magnitude of the long-term inter-species interaction coefficient (a_{ij}). **d**, Representative community dynamics of *C. difficile* and gut bacteria in pairwise (left) and three-member (right) communities to show stable coexistence, unstable coexistence, and competitive exclusion. Dots connected by colored lines indicate the relative abundance of each species (left y-axis) whereas the grey lines with shaded 95% confidence interval (CI) indicate the community OD_{600} (right y-axis). The complete community dynamics are shown in **Fig. S1c-d**. **e**, Measurement of the degree of coexistence (ΔH) using the Shannon diversity at the last time point relative to the initial time point in all pairwise and three-member communities containing the specific species shown in the x-axis. Horizontal dashed line indicates a value of 1 (Shannon diversity at the last time point is equal to the initial time point). The complete Shannon diversity throughout the passages is available in **Fig. S4**. **f**, Box plot of Euclidean distances between time point measurements throughout 35 passages in all pairwise and three-member communities containing the specific species shown in the x-axis. For **panel e-f**, the number of data points is shown below the plots.

   C. difficile persisted in 60% of the communities (7/9 pairwise and 20/36 three-member communities) (**Fig. S1c-d**). However, the absolute abundance of *C. difficile* decreased from the initial to the final passage in 84% of communities (**Fig. S2a**). Certain species, such as PC and BT, were enriched in communities that displayed substantial *C. difficile* inhibition. To quantify the impact of human gut species on the long-term growth

158   of *C. difficile*, we fit a generalized Lotka–Volterra (gLV) model to the time-series data of
159   species abundances (over 35 passages) of monoculture, pairwise, and three-member
160   communities by simulating the passaging experimental design (**Fig. 1b**, DATASET001 in
161   **Table S3**, **Methods**). The gLV model is a dynamic ecological model that can predict
162   community dynamics as a function of each species' growth and pairwise interactions with
163   all constituent community members. This model has been used extensively to decipher
164   inter-species interactions and predict community assembly across different environments
165   [14,52,60,61]. The inferred gLV inter-species interaction coefficients quantify the effect of a
166   given species on the long-term growth of another species. The model shows good
167   prediction performance on the measured species abundances across passages
168   (Pearson's R=0.89-0.91, P=3.6E-42 to 2.3E-51) (**Fig. S3a-b**).

169   In contrast to inferred gLV inter-species interaction networks dominated by
170   negative interactions based on short timescales [55], the inferred network for long-term
171   ecological interactions displayed a high frequency of positive interactions (**Fig. 1c**).
172   Certain species, such as PV and DP, displayed bidirectional positive interactions with *C.*
173   *difficile* over this timescale that can destabilize community dynamics based on theoretical
174   studies [62-64] (**Fig. 1d, S1c-d**). By contrast, EL displayed an outgoing positive and incoming
175   negative interaction with *C. difficile*. This topology generates a negative feedback loop
176   that can stabilize community dynamics [60], providing insights into the observed stable
177   coexistence between EL and *C. difficile* (**Fig. S1c**). Previous studies showed potential
178   inhibitory effects of CH and CS on *C. difficile* [14,55,65-69], consistent with the inhibition of *C.*
179   *difficile* by CH inferred by the model. However, CH and CS were outcompeted by *C.*
180   *difficile* in pairwise co-culture after 7 passages and were frequently excluded from the 3-
181   member communities (**Fig. S1c-d, S2b**). Therefore, interventions that enhance the
182   abundance of CH and CS in human gut communities may be critical to achieving robust
183   inhibition of *C. difficile* over long timescales.

184   To evaluate the degree of coexistence in the community, we calculated the change
185   in Shannon diversity over time (ΔH) (**Fig. 1e, S4**). Communities containing EL displayed
186   the highest ΔH, whereas communities containing BT displayed the lowest ΔH. In addition,
187   we quantified the extent of variability in community dynamics using the Euclidean distance
188   of species' relative abundances between each pair of time points. Large values of
189   Euclidean distance indicate community instability, whereas small values indicate
190   temporal stability. The presence of PV and DP yielded larger Euclidean distances than
191   other species (**Fig. 1f**), consistent with their bidirectional positive interaction network
192   topology.

193   We investigated community dynamics of a subset of communities that displayed
194   coexistence with *C. difficile* over longer timescales and across different environmental
195   conditions. Specifically, we cultured pairwise communities containing CA, EL, BU, DP,
196   and PV with two distinct *C. difficile* strains in three different media conditions for 341
197   generations (**Fig. S5a-d**). Since *C. difficile* has large genetic variability across strains [70-
198   73], we characterized a toxigenic DSM 27147 strain and a non-toxigenic MS001 strain with
199   a larger genome and distinct metabolic capabilities [55]. In addition, we analyzed three
200   nutrient environments: DM, DM with a 4-fold lower carbohydrate concentration, and DM

201 with a 2-fold higher amino acid concentration. Decreasing the concentration of
202 carbohydrates could influence *C. difficile* growth by altering the strength of competition
203 and/or media acidification by certain gut species. Increasing amino acid availability could
204 enhance the growth of *C. difficile* due to Stickland metabolism [74]. Overall, *C. difficile* DSM
205 and MS001 displayed similar long-term dynamics across communities and nutrient
206 environments except in co-culture with PV in DM and DM with increased amino acids,
207 and with DP in DM with limited carbohydrates (**Fig. S5e-g**). The dynamics of CD-PV and
208 CD-DP exhibited larger instability (**Fig. S5h-j**) and displayed larger variation across the
209 distinct nutrient environments than other communities (**Fig. S5e-g**).

210 The long-term growth dynamics of *C. difficile* with PV or DP displayed qualitative
211 differences across different experiments when cultured via serial dilutions in the same
212 media (DM) (**Fig. S1c, S5e**). For instance, while species relative abundance alternated
213 between high and low values across 35 passages in the CD-PV community in one
214 experiment (**Fig. S1c**), *C. difficile* was excluded from the community between the 35th to
215 42nd passage in a different experiment (**Fig. S5e**). This suggests that the observed
216 instability in community dynamics yielded an elevated risk of extinction, consistent with
217 previous theoretical studies [45]. This variability in growth dynamics was also observed
218 across biological replicates containing CD and PV (e.g. in CD-PV-CS), where one
219 replicate displayed unstable coexistence and another displayed competitive exclusion.

220 In sum, certain species such as EL promote stable coexistence of *C. difficile* in
221 communities across long timescales. By contrast, PV or DP promotes instability in
222 community dynamics across different environmental conditions. These dynamics are
223 overall consistent with their inferred interaction network topologies.

224

225 *Resource-limited environment promotes metabolite cross-feeding and coexistence*
226 *between C. difficile and P. vulgatus*

227 Previous studies have shown that 30% of bacteria in the human colon are *Bacteroides*
228 species, with PV, BT, BU*, B. distasonis, B. fragilis*, and *B. ovatus* displaying the highest
229 prevalence across individuals [75-78]. Studying interactions between *C. difficile* and these
230 highly abundant and prevalent species could provide insights into the factors shaping *C.*
231 *difficile* colonization. CD-PV co-culture displays a unique feature where modifying the
232 nutrient environment could alter community dynamics from competitive exclusion to
233 coexistence over this timeframe (**Fig. S5e-f**). In the presence of high carbohydrate
234 concentrations, *C. difficile* was excluded between ~186-224 generations, whereas in
235 media with reduced carbohydrate concentration, *C. difficile* coexisted with PV over 341
236 generations.

237 To uncover the metabolic activities driving coexistence versus competitive
238 exclusion in these conditions, we performed exo-metabolomic profiling on PV and *C.*
239 *difficile* in both media (**Fig. 2a-b**). In the limited carbohydrate media, our results were
240 consistent with the cross-feeding of multiple metabolites from PV to *C. difficile* (**Fig. 2a,**

241 **S6**). In monoculture, *C. difficile* consumed many amino acids in the media due to its ability
242 to perform Stickland metabolism [65,74,79,80]. Notably, PV released 84% of the metabolites
243 that *C. difficile* utilized, including amino acids for Stickland metabolism. These metabolites
244 displayed a larger decrease in abundance in the CD-PV co-culture than in the PV
245 monoculture, suggesting that they are being consumed by *C. difficile*. The release of
246 amino acids and cross-feeding from *Bacteroides* to *Clostridium* species has been
247 previously reported [81,82]. By contrast, the predicted cross-feeding is sparse in the high
248 carbohydrate media where 12% of the metabolites that *C. difficile* utilized were released
249 by PV (**Fig. 2b, S7**). This is consistent with a previous study where high concentrations
250 of acetate suppressed the release of many metabolites from *Bacteroides* including amino
251 acids [83]. Further, 24% of the metabolites that *C. difficile* consumed are also consumed by
252 PV in monoculture, implying a higher degree of resource competition in this environment.
253 In this media, both *C. difficile* and PV utilized glucose and inositol. Of the metabolites that
254 *C. difficile* consumed in the high carbohydrate media, 45% were also consumed in the
255 limited carbohydrate media.

256
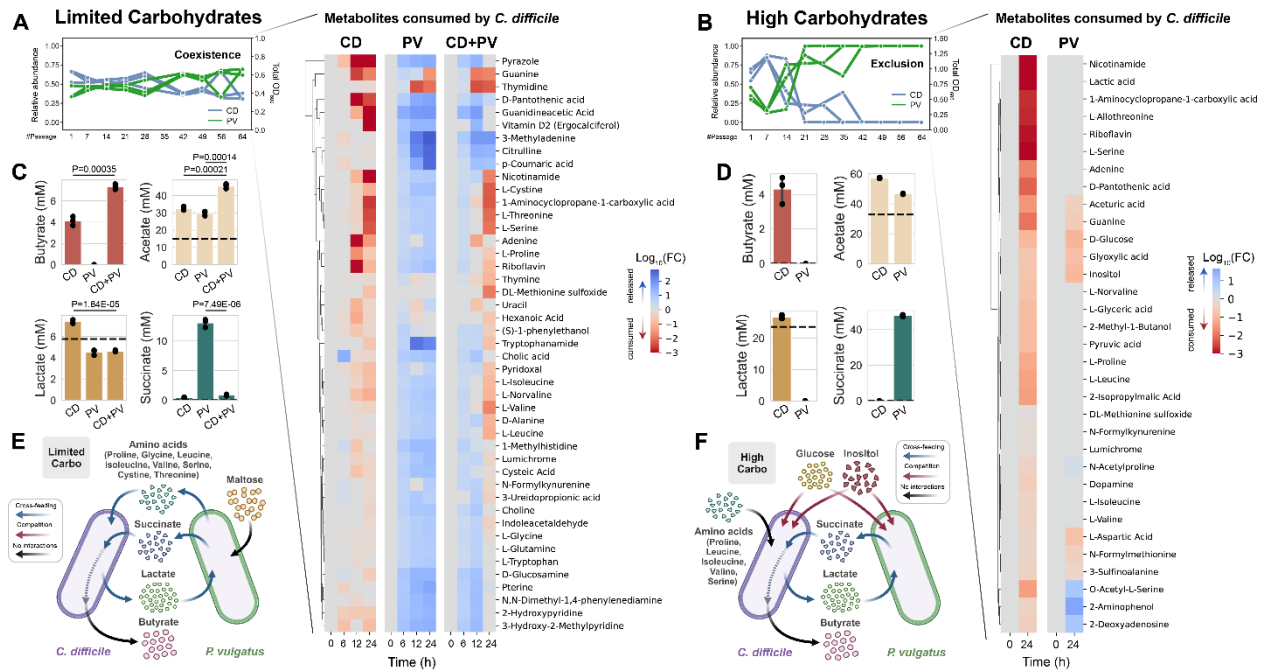
258 **Figure 2. Exo-metabolomic profiling of *C. difficile* and PV in two media conditions. a-b**,
259 Heatmap of the fold change of metabolites consumed by *C. difficile* in DM with reduced
260 carbohydrate concentration (limited carbohydrate media) (**a**) or DM (high carbohydrate media) (**b**)
261 compared to the blank media (t = 0 h). The complete metabolomics profile is shown in **Fig. S6** for
262 DM with limited carbohydrates and **Fig. S7** for DM. The figures of the time-course abundance
263 measurement were taken from **Fig. S5e** and **f**. **c-d**, Quantification of organic acids in DM with
264 reduced carbohydrate concentration (**c**) and DM (**d**) (mean ± s.d., n=3). Horizontal dashed lines
265 indicate the concentration detected in the blank media. The *p*-values from unpaired *t*-test (two-
266 sided) are shown. **e-f**, Schematic of major metabolic activities in CD-PV co-culture in DM with

267 reduced carbohydrate concentration (**e**) and DM (**f**). Parts of the figure are generated using
268 Biorender.

270   By performing exo-metabolomics on the other 8 human gut species in
271 monocultures, our results suggested that potential cross-feeding is unique to the PV-CD
272 community in the limited carbohydrate media. Specifically, only ~3-15% of the metabolites
273 released by other gut species were utilized by *C. difficile* (**Fig. S7a-c, f**). Of the 9 gut
274 bacteria, CS and CH have the highest metabolite utilization overlap with *C. difficile* and
275 could compete with *C. difficile* over Stickland amino acids [65,84]. This potential resource
276 competition is consistent with their extinction in co-culture with *C. difficile* (**Fig. S1c**). CS
277 and CH also have lower growth rates than *C. difficile* (**Fig. S8a-c**). In addition to cross-
278 feeding, the coexistence of species can be mediated via the utilization of unique
279 resources [85]. Of all metabolites consumed by *C. difficile* in the high carbohydrate media,
280 21% are unique (**Fig. S7f**). This implies that orthogonal niches may enable the
281 coexistence of *C. difficile* with certain gut species in this media, such as CA, BU, and EL
282 (only 9%, 15%, and 21% metabolite utilization overlap respectively) (**Fig. 1e, S1c-d**). The
283 number of metabolites consumed by *C. difficile* was the second largest after CS (**Fig.
284 S7d**), suggesting that *C. difficile* has a flexible metabolic niche.

285   Fermentation end products play key roles in inter-species interactions in the
286 human gut microbiome [86]. Therefore, we quantified the concentration of butyrate, lactate,
287 acetate, and succinate in the supernatants of *C. difficile* and PV after 24 h of growth (**Fig.
288 2c-d**). While acetate was produced by *C. difficile* and PV, PV produced succinate, and *C.
289 difficile* produced butyrate in both media conditions. In co-culture, succinate produced by
290 PV was substantially reduced, and butyrate produced by *C. difficile* was higher than in
291 monoculture (**Fig. 2c**). This implies that *C. difficile* used succinate released by PV to
292 produce butyrate [74]. Cross-feeding of succinate from *Bacteroides* to *C. difficile* has also
293 been observed in mice, suggesting that this metabolic exchange is relevant for the
294 mammalian gut [56]. In addition, *C. difficile* produced lactate that was consumed by PV in
295 monoculture and co-culture (**Fig. 2c-d**). In sum, these data suggest that PV and *C. difficile*
296 can interact via metabolite exchange of multiple metabolites.

297   Overall, an environment with limited carbohydrates promotes metabolite cross-
298 feeding and coexistence between *C. difficile* and PV (**Fig. 2e**). In the presence of high
299 carbohydrate concentrations, resource competition may dominate over cross-feeding,
300 thus promoting the exclusion of *C. difficile* in co-culture with PV after ~35-42 passages
301 (**Fig. 2f**). In addition, *C. difficile* uniquely consumes a subset of metabolites in this media,
302 which could contribute to the observed coexistence with other human gut species such
303 as CA and EL.

305 *Evolutionary adaptations of C. difficile in co-culture with PV leads to altered metabolic*
306 *activities*

307　Prolonged coexistence between *C. difficile* and PV could lead to evolutionary adaptations
308　in *C. difficile*. In the limited carbohydrate media, *C. difficile* abundance decreased over
309　time (**Fig. S5f, 2a**). To determine if the change in abundance stemmed from an
310　evolutionary adaptation, we isolated *C. difficile* from the final passage of the CD-PV
311　community. The isolated *C. difficile* strain (evolved strain) displayed a lower relative
312　abundance than the ancestral strain in co-culture with PV in the media used to isolate the
313　strain (**Fig. S9a**). Notably, when co-cultured with PV over 341 generations in the limited
314　carbohydrate media, the evolved *C. difficile* strain displayed a converging trend towards
315　approximately equal species proportion, whereas the abundance of the ancestral strain
316　was diverging away from equal proportions (**Fig. S9b-c**). This implies that the evolved *C.*
317　*difficile* strain could coexist better with PV than the ancestral strain over this timescale.

318　　　　Whole-genome sequencing (WGS) revealed that the isolated *C. difficile* strain
319　harbored two single-point non-synonymous mutations (**Fig. 3a, Table S4**). The mutations
320　are located in *gene 206* (G533W) expressing the phosphotransferase system (PTS)
321　sugar transporter subunit IIA, and in *prdR* (A341V), a central metabolism regulator that
322　controls preferential utilization of proline and glycine to produce energy via the Stickland
323　reactions. In the presence of proline, PrdR activates transcription of the proline reductase-
324　encoding genes and negatively regulates the glycine reductase-encoding genes [79].
325　Sanger sequencing of the *prdR* gene confirmed the presence of A341V mutation in *C.*
326　*difficile* isolated from two other biological replicates of the CD-PV pair. This mutation was
327　not present in other pairwise communities (CD-BU, CD-CA, CD-DP, CD-EL) or *C. difficile*
328　that was passaged alone in the same media condition, suggesting that the mutation
329　uniquely emerged in co-culture with PV. By subjecting the whole CD-PV population to
330　WGS, we also detected the mutation in *gene 206* (G533W) in *C. difficile* across all three
331　biological replicates of the CD-PV pairwise community. In addition, we identified several
332　mutations arising in PV's genome in the CD-PV pairwise community that did not reach
333　fixation by the 64th passage (~18 to 46% of the population) (**Table S5**). Notably, some of
334　the genes with identified non-synonymous mutations were frequently mutated in
335　*Bacteroides* in healthy humans [87].

336
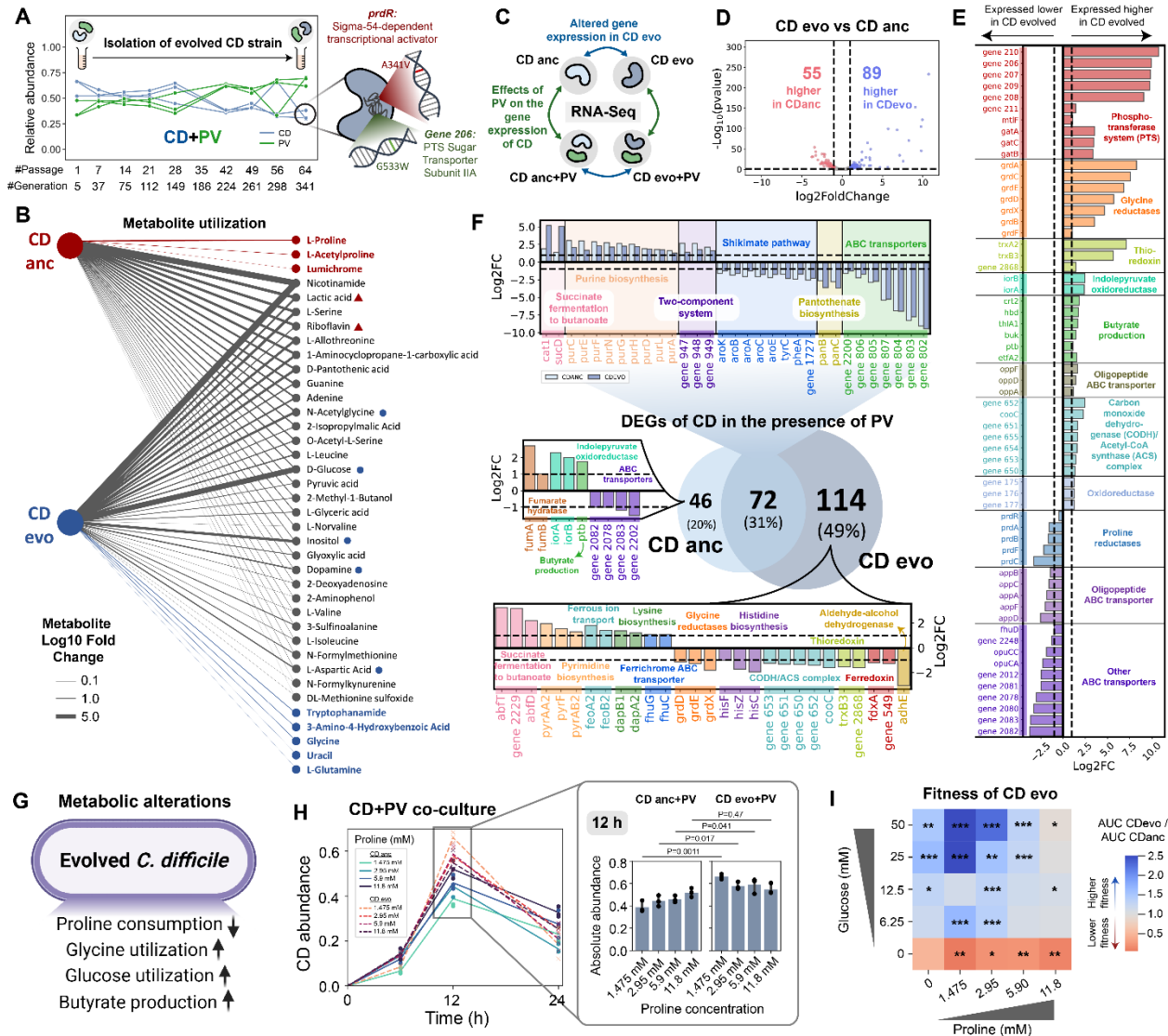
Figure 3. *C. difficile* **undergoes evolutionary adaptations that alter its metabolism after prolonged co-culture with** *P. vulgatus*. **a**, *C. difficile* was isolated from CD-PV grown in limited carbohydrate media after 341 generations. Figure of the community dynamics was taken from **Fig. S5f**. **b**, Bipartite network of metabolite utilization between the ancestral and evolved *C. difficile* strains in DM. Metabolites shown have significantly lower concentrations than the blank media (two-sided t-test with unequal variance). Metabolites bolded with red (blue) are uniquely utilized by the ancestral strain (evolved strain). Metabolites marked with red triangle (blue circle) asterisks have >10-fold higher utilization in the ancestral strain (evolved strain). **c**, Schematic of the genome-wide transcriptional profiling experiment. **d**, Volcano plot of log-transformed transcriptional fold changes of the evolved *C. difficile* strain compared to the ancestral strain. Vertical dashed lines indicate 2-fold change and horizontal dashed line indicates the statistical significance threshold as calculated by DESeq2's Wald test with Benjamini-Hochberg multiple testing correction (BH-adjusted p=0.05). **e**, Log-transformed fold changes of selected genes that were expressed higher and lower in the evolved *C. difficile* strain compared to the ancestral strain. Vertical dashed lines indicate a 2-fold change. **f**, Comparison of DEGs in the ancestral and evolved *C. difficile* strains in the presence of PV. **g**, Schematic of metabolic alterations in the evolved *C. difficile* strain. **h**, *C. difficile* abundance when grown with PV under different proline

355 concentrations. Solid (dashed) lines indicate ancestral (evolved) *C. difficile* strain when co-
356 cultured with PV. Bar plots show *C. difficile* abundance at 12 h (mean ± s.d., n=3). *p*-values from
357 unpaired *t*-test (two-sided) between evolved and ancestral strains are shown. **i**, Heatmap of
358 fitness of the evolved *C. difficile* strain compared to the ancestral strain in response to varying
359 glucose and proline concentrations. Fitness comparison is quantified by the Area Under the Curve
360 (AUC) ratio based on monoculture growth (**Fig. S14**). Asterisks indicate *p*-value from unpaired *t*-
361 test between evolved and ancestral strains. *** indicates p<0.001, ** indicates p<0.01, * indicates
362 p<0.05, ns indicates not significant. Exact p-values are shown in **Fig. S14**. Parts of the figure are
363 generated using Biorender.

364

365   Since these mutations could impact metabolic activities, we characterized the
366 difference in exo-metabolomic profile of the evolved and ancestral *C. difficile* strains in
367 the high carbohydrate media (DM) (**Fig. 3b, S10**) and limited carbohydrate media (**Fig.**
368 **S6**). While the ancestral strain consumed proline consistent with previous knowledge of
369 its metabolism [55,79], proline in DM was not significantly reduced by the evolved strain (**Fig.**
370 **3b**). By contrast, the consumption of glycine, aspartic acid, and N-acetylglycine (a
371 derivative of glycine) was enhanced by the evolved strain. Similarly, in the limited
372 carbohydrate media, the evolved *C. difficile* strain displayed a reduced rate of proline
373 utilization compared to the ancestral strain both in monoculture and co-culture with PV
374 (**Fig. S6d**). By contrast, the consumption rate of many other amino acids including glycine,
375 leucine, isoleucine, valine, and serine was higher in the evolved *C. difficile* strain both in
376 monoculture and co-culture with PV. In addition to amino acids, the evolved strain
377 consumed more glucose than the ancestral strain in both media conditions.

378   To provide insights into how the mutations affect the gene expression of *C. difficile,*
379 we performed genome-wide transcriptional profiling on the ancestral and evolved *C.*
380 *difficile* strains in the absence and presence of PV (**Fig. 3c, S11a-b**). Since one of the
381 mutations plays a role in carbohydrate utilization, we cultured cells in DM where *C. difficile*
382 consumed glucose and inositol in addition to amino acids (**Fig. 2f**). Of 3,508 total genes,
383 89 and 55 displayed significantly higher and lower expression respectively in the evolved
384 *C. difficile* than the ancestral strain in monoculture (**Fig. 3d-e, Table S6**). PTS-related
385 genes, including the mutated gene 206, were expressed substantially higher in the
386 evolved strain. This suggests that the evolved strain adapted to transport and
387 phosphorylate carbohydrates more effectively than the ancestral strain, contributing to
388 the observed higher utilization of carbohydrates such as glucose (**Fig. 3b**). Although the
389 change in *prdR* expression was moderate (1.4-fold up-regulated), there was a massive
390 shift in the expression of the *prd* and *grd* operon. Specifically, the glycine reductase-
391 encoding genes were highly up-regulated (2.1-305-fold), whereas the proline reductase-
392 encoding genes were down-regulated (3.0-9.7-fold) in the evolved strain compared to the
393 ancestral (**Fig. 3e**). This is consistent with the alterations in proline and glycine utilization
394 in the evolved strain as observed through exo-metabolomic profiling (**Fig. 3b, S6d**).

395   Other metabolic genes such as the carbon monoxide dehydrogenase/acetyl-CoA
396 synthase complex that is responsible for the carbonyl branch of the Wood–Ljungdahl

397   Pathway (WLP), converting CO_2 to acetyl-CoA, were expressed higher in the evolved
398   strain compared to the ancestral (**Fig. 3e**). In the evolved strain, genes for butyrate
399   production including *thlA1, hbd, crt2* (converting acetyl-CoA to butyryl-CoA) and *ptb* and
400   *buk* (converting butyryl-CoA to butyrate), were also expressed higher. The evolved strain
401   displayed 2.7-fold higher butyrate production than the ancestral strain (**Fig. S12a**). This
402   higher level of butyrate produced by the evolved *C. difficile* strain (11.6 mM) is comparable
403   to a major butyrate-producing bacteria *Coprococcus comes* cultured in a similar media
404   [51,88] and could potentially influence disease severity *in vivo* [89]. Previous studies have
405   shown that certain *Bacteroides* species displayed nutrient-specific growth sensitivity
406   towards butyrate [90]. Of the characterized *Bacteroides* species, only PV displayed
407   significant growth reduction under intermediate butyrate concentrations. The butyrate
408   concentration produced by the evolved strain was in the lower-inhibitory regime of the
409   butyrate dose-response curve for PV (**Fig. S12b**).

410   In co-culture with PV, both the ancestral and evolved *C. difficile* strains up-
411   regulated genes for succinate fermentation to butanoate, with the evolved strain exhibiting
412   higher expression of these genes (**Fig. 3f**, **S11c-f, Table S7-9**). Since the growth media
413   does not contain succinate, this implies cross-feeding from PV, consistent with the
414   organic acids measurements data (**Fig. 2c-d**). The gene expression profile of PV also
415   displayed substantial differences in co-culture with the ancestral and evolved *C. difficile*
416   strain. Notably, PV exhibited higher expression of many genes involved in amino acid
417   biosynthesis in the presence of the evolved *C. difficile* strain compared to the ancestral
418   strain (**Fig. S11g**). This indicates that PV's amino acid biosynthesis is either induced by
419   the evolved *C. difficile* strain or inhibited by the ancestral strain, which might contribute to
420   the observed differences in the long-term growth dynamics between the ancestral and
421   evolved *C. difficile* strain with PV (**Fig. S9b**). Since the evolved *C. difficile* strain has a
422   higher consumption of many amino acids (**Fig. S6d**), this implies an enhanced strength
423   of amino acid cross-feeding with PV, providing insights into a mechanism that may
424   enhance stable coexistence with PV (**Fig. S9b**).

425   Overall, evolutionary adaptations that altered *C. difficile* metabolism (**Fig. 3g**) and
426   increased its ability to coexist with PV (**Fig. S9b**) arose after prolonged coexistence with
427   PV.

428

Growth of evolved C. difficile strain is less limited by proline and enhanced in the presence
of high glucose concentrations

431   A key unresolved question is how this metabolic adaptation impacts the fitness of *C.*
432   *difficile* across different environments. To evaluate changes in fitness, we characterized
433   the growth of the evolved and ancestral *C. difficile* strains in the presence of different
434   amino acid concentrations. The evolved *C. difficile* strain displayed higher growth than
435   the ancestral strain in the presence of reduced amino acid concentrations (20%) at earlier
436   time points, whereas the growth responses of the two *C. difficile* strains were similar in

437 other conditions (**Fig. S9d**). The EC$_{50}$ of the evolved *C. difficile* strain for proline
438 (concentration of proline that yields 50% of the maximum growth) was substantially lower
439 than the ancestral strain (**Fig. S13a, e**). This indicates that the evolved strain can compete
440 more efficiently for low proline concentrations than the ancestral strain. Proline is the
441 growth-limiting resource for the ancestral *C. difficile* strain in our media, which has been
442 observed in many other *C. difficile* clinical isolates with diverse genomes [55]. However,
443 proline is not the limiting substrate for the evolved strain as evidenced by our
444 metabolomics data (**Fig. 3b**). Consistent with this result, the abundance of the evolved
445 strain did not vary with proline in co-culture with PV, indicating that the growth of the
446 evolved *C. difficile* strain was in the saturated regime of proline concentrations (**Fig. 3h,
447 S13g**). By contrast, the abundance of the ancestral strain increased with proline
448 concentration (i.e. linear regime of proline dose-response). The abundance of the evolved
449 *C. difficile* strain was higher than the ancestral strain in co-culture with PV at 12 h under
450 low initial proline concentration and then decreased to the final time point (**Fig. 3h**). The
451 evolved and ancestral strains displayed similar growth as a function of glycine in
452 monoculture (**Fig. S13b, d**) and in co-culture with PV (**Fig. S13h**).

453 The glucose EC$_{50}$ of the evolved *C. difficile* strain was higher than the ancestral
454 strain (**Fig. S13f**). In addition, the evolved strain displayed higher biomass than the
455 ancestral strain under high glucose concentrations (**Fig. S13c, f**), but similar size and
456 morphology at the single-cell level (**Fig. S9e**). This implies that the evolved strain more
457 efficiently utilizes high glucose concentrations. In the low-concentration regime, the
458 evolved *C. difficile* strain displayed a trade-off between increased sensitivity towards
459 proline and reduced utilization of glucose. In co-culture with PV, the evolved *C. difficile*
460 strain displayed lower abundance than the ancestral strain at low glucose concentrations
461 but displayed similar growth at high glucose concentrations (**Fig. S13i**). This is consistent
462 with its reduced growth compared to the ancestral strain in the presence of PV in the
463 limited carbohydrate media (**Fig. S9a**).

464 In sum, the shift in metabolic activities in the evolved *C. difficile* strain (**Fig. 3g**)
465 impacts its fitness across different combinations of proline and glucose. The fitness of the
466 evolved strain was enhanced in the presence of high glucose and low proline
467 concentrations, whereas the ancestral strain displayed higher fitness in the absence of
468 glucose and the presence of proline (**Fig. 3i, S14**).

469

470 *Evolved C. difficile strain displayed altered inter-species interactions with human gut*
471 *bacteria*

472 To investigate whether the observed metabolic shifts in the evolved *C. difficile* strain
473 impact human gut microbiota inter-species interactions, we constructed 96 combinations
474 of 2-8 member communities containing the evolved or the ancestral *C. difficile.* The other
475 species span the phylogenetic diversity of the human gut microbiome, are highly
476 prevalent across the human population (CS, CH, DP, BT, PV, BU, and CA), and have

477   been extensively characterized in different media (**Fig. 4a**) [14,55,60]. We fit the gLV model
478   to the time-series data of species absolute abundances (0, 12, and 24 h) (**Table S3**
479   DATASET002, **Fig. S15a-c**). To evaluate model prediction performance on held-out data,
480   we performed 10-fold cross-validation where the model was trained on a fraction of the
481   data and then used to evaluate prediction performance on the held-out community
482   measurements (**Fig. S15d,** see **Methods**). Using a 10-fold cross-validation, the model
483   prediction exhibited good agreement with the measured species abundance in all
484   communities containing the ancestral and the evolved *C. difficile* strain (Pearson's
485   R=0.95-0.99, P<10E-05). However, certain species such as CH, displayed a low to
486   moderate prediction performance [55]. This might be due to insufficient variation of the
487   particular species abundance across communities or limited flexibility of the gLV model
488   to capture complex interaction modalities [91].

489
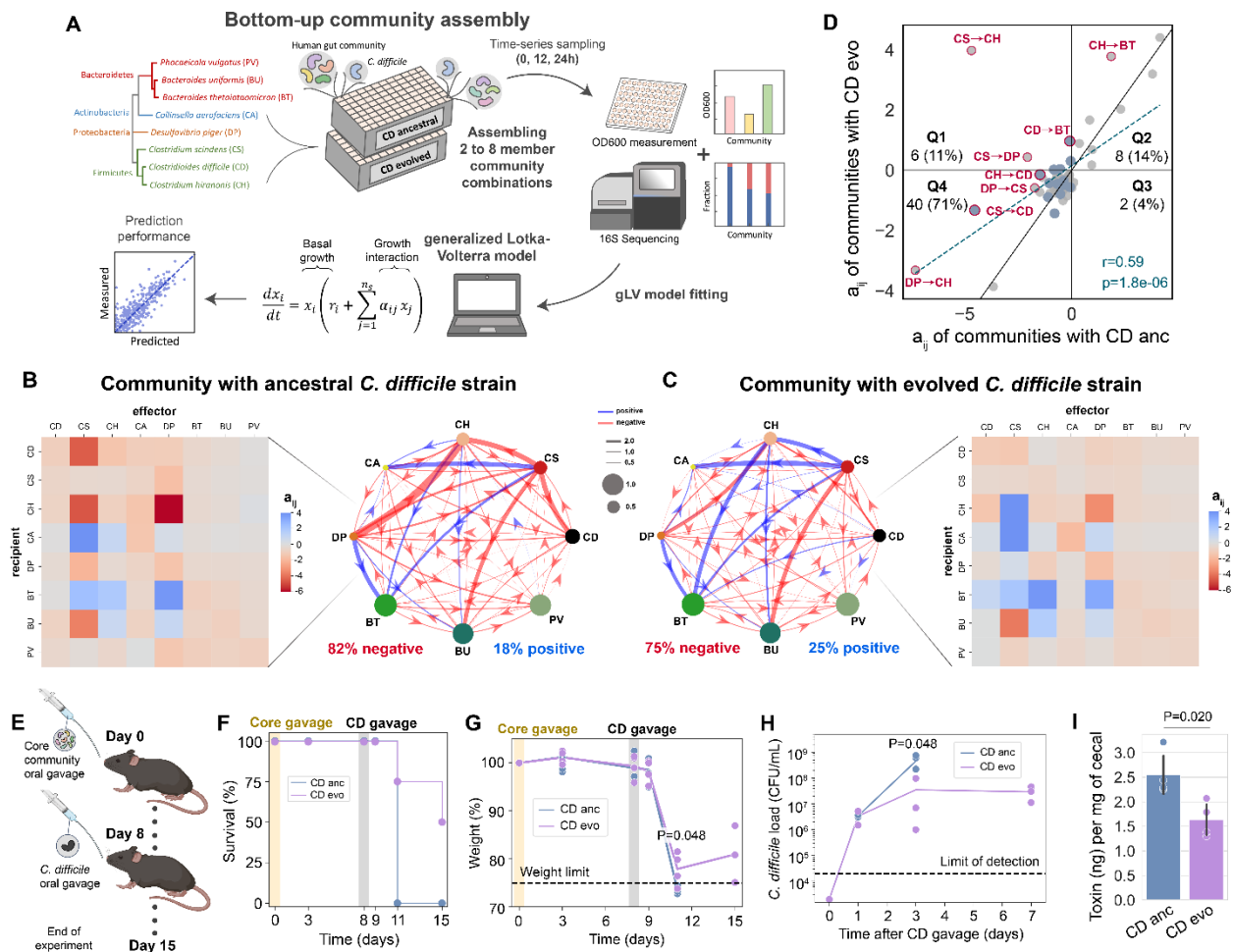
491   **Figure 4. Evolved *C. difficile* strain displayed alteration in inter-species interactions with**
492   **human gut bacteria and reduced disease severity in the mammalian gut. a**, Schematic of
493   workflow to decipher interactions between ancestral and evolved *C. difficile* strain and human gut
494   bacteria (See **Methods, Table S3** DATASET002). The gLV model was fit to species absolute

495 abundance and the inferred gLV parameters revealed inter-species interactions. **b-c**, Inferred
496 inter-species interaction networks between the 7 gut species and the ancestral (**b**) and evolved
497 (**c**) *C. difficile* strain. Node size represents species carrying capacity and edge width represents
498 the magnitude of the inter-species interaction coefficient (a_{ij}). The heatmaps show the a_{ij} among
499 the 8 species in the community. **d**, Scatter plot of the a_{ij} between communities containing ancestral
500 versus evolved *C. difficile* strain. Grey data points are a_{ij} between two gut species, whereas blue
501 data points are a_{ij} between *C. difficile* and a gut species. Blue dashed line indicates linear
502 regression between the a_{ij} values of the two communities. Two-sided Pearson's correlation
503 coefficient (*r*) and *p*-values are shown. **e**, Schematic of the mice experiment. Mice were gavaged
504 with a 7-member bacterial community for 8 days prior to challenge with the ancestral or evolved
505 *C. difficile* strain. **f**, Percent survival of mice gavaged with ancestral and evolved *C. difficile* strain.
506 **g**, Percent of initial weight of mice gavaged with ancestral and evolved *C. difficile* strain. Data
507 points indicate individual mice, and the line indicates the average of all mice in the group.
508 Horizontal dashed line indicates the weight limit of 75%. Mice with weights that dropped below
509 the limit were sacrificed. **h**, *C. difficile* load in the fecal (survived mice) and cecal (dead mice)
510 content as determined by CFU counting on *C. difficile* selective plates. Horizontal dashed line
511 indicates limit of detection. For panel **g-h**, significant *p*-values from unpaired *t*-test (two-sided)
512 between mice gavaged with ancestral vs. evolved *C. difficile* strain are shown. **i**, Toxin
513 concentration per mg of cecal content. Data were shown as mean ± s.d. (n=4). *p*-value from
514 unpaired *t*-test (two-sided) is shown. Parts of the figure are generated using Biorender.

515

516   Based on the inferred gLV parameters, both pairwise interaction networks
517 displayed a high frequency of negative interactions, consistent with previous findings [14,55]
518 (**Fig. 4b-c**). The frequency of positive interactions in the community was higher in the
519 presence of the evolved (25%) versus ancestral (18%) *C. difficile* strains. In addition, 15%
520 of inter-species interactions displayed inconsistent signs in the evolved versus ancestral
521 inter-species interaction network (**Fig. 4d**). This implies that the two single-point
522 mutations in the evolved strain are critical determinants of gut microbiota inter-species
523 interactions. While CS and CH strongly inhibited the ancestral *C. difficile's* growth, this
524 inhibition is substantially suppressed for the evolved *C. difficile* strain. Since the evolved
525 *C. difficile* strain uses more glucose and less proline (**Fig. 3b**), this could relieve the
526 competition over proline with CS and CH. Beyond pairwise interactions between *C.*
527 *difficile* and gut species, the evolutionary adaptations of *C. difficile* also indirectly impacted
528 pairwise interactions between other constituent community members, mainly CS and CH
529 with other gut species (**Fig. 4d**). Overall, *C. difficile's* evolutionary adaptation yielded
530 substantial direct and indirect alterations of human gut microbiota inter-species
531 interactions. These changes could emerge due to the shifts in the metabolic niche of the
532 evolved *C. difficile* strain (**Fig. 3, S6, S10**).

533

534 *Evolved C. difficile strain reduced disease severity in the mammalian gut*

535 Amino acids such as proline have been shown to regulate *C. difficile* toxin production *in*
536 *vitro* [79,92-94] and influence colonization in the mammalian gut [80,95]. To determine if the *C.*
537 *difficile* evolutionary adaptations alter toxin production, we characterized toxin expression
538 using the Enzyme-Linked Immunosorbent Assay (ELISA) after 24 h of growth. The

539 evolved *C. difficile* strain displayed substantially lower toxin concentration and yield (toxin
540 concentration divided by the OD_{600} of *C. difficile*) compared to the ancestral strain across
541 a wide range of amino acid concentrations (**Fig. S16**).

542   To examine whether the metabolic adaptations in the evolved *C. difficile* strain
543 impact disease severity, we orally gavaged germ-free mice with the 7-member synthetic
544 human gut community (CS, CH, DP, BT, PV, BU, and CA) for 8 days to allow time for the
545 establishment of a stable human gut community and immune system training [96] (**Fig. 4e**).
546 After 8 days, a group of mice was orally gavaged with the ancestral *C. difficile* strain, and
547 another group was gavaged with the evolved *C. difficile* strain. Three days after *C. difficile*
548 inoculation, all the mice gavaged with the ancestral *C. difficile* strain died (**Fig. 4f-g**). By
549 contrast, only 50% of the mice harboring the evolved *C. difficile* strain died after 3 and 7
550 days of *C. difficile* colonization. The relative reduction in weight for mice harboring the
551 evolved *C. difficile* strain was significantly lower than the mice harboring the ancestral *C.*
552 *difficile* strain, although both groups displayed a decreasing trend in weight over the first
553 few days after *C. difficile* challenge. After 3 days of *C. difficile* challenge, the mean fraction
554 of the ancestral and evolved *C. difficile* strain in the community was 10.6% and 3.3%
555 respectively (**Fig. S17**). Mice gavaged with the evolved *C. difficile* strain displayed
556 significantly lower *C. difficile* abundance and toxin concentration compared to the mice
557 gavaged with the ancestral *C. difficile* strain (**Fig. 4h-i**). In sum, the evolved *C. difficile*
558 strain displayed reduced colonization ability and reduced disease severity in the murine
559 gut compared to the ancestral *C. difficile* strain.

560

561 *Nutrient environments impact variability in long-term community assembly*

562 Community dynamics have different degrees of stability over the passages (**Fig. 1f, S5h-**
563 **j**), and higher instability leads to larger variability. Characterizing the growth of *C. difficile*
564 in communities over long timescales across a larger number of replicates could provide
565 insights into how composition diffuses over periodic regrowth cycles due to variability in
566 growth dynamics [41]. Understanding the factors that modulate variability in community
567 assembly is important as it could influence the ability of *C. difficile* to persist in the
568 community over time. To evaluate the degree of variability in *C. difficile* growth within a
569 community after long-term passaging, *C. difficile* was introduced into an 8-member
570 community with 96 biological replicates (**Fig. S18a**). *C. difficile* persisted in the community
571 with a nearly constant mean of absolute abundance, but the variability in abundance
572 across replicates substantially increased from the first to the 14th passage and then
573 increased again from the 42nd to the 56th passage (**Fig. S18c-e**).

574

Figure 5. Nutrient environments shape the variability of long-term community assembly. a, Stacked bar plot of the absolute abundance (OD_{600}) of the independent replicates of 2, 4, and 6-member community containing *C. difficile* over 49 passages grown in media containing only glucose (**left**) or multiple *C. difficile*-preferred carbohydrates (**right**). Two-member communities were grown with 12 independent replicates, whereas 4 and 6-member communities were grown with 24 independent replicates. Contaminated replicates were excluded from the analysis. **b**, Euclidean distance of community composition between pairs of replicates from the 1st to the 49th passages in the two media conditions. *p*-values from unpaired *t*-test (two-sided) between different sample groups are shown. **c**, Coefficient of variations of *C. difficile* abundance across replicates from the 1st to the 49th passages in the two media conditions. The *p*-value from unpaired *t*-test (two-sided) of the coefficient of variations between the two media conditions is shown.

The impact of environments with multiple *C. difficile*-preferred carbohydrates versus glucose as a single highly accessible resource on gut microbiota inter-species

590 interactions with *C. difficile* has been studied [55], but their role in shaping the variability of
591 *C. difficile* growth is not known. We cultured *C. difficile* with human gut communities in
592 the presence of glucose as a single highly accessible resource or multiple *C. difficile*-
593 preferred carbohydrates mirroring post-antibiotic environments where numerous
594 resources could be exploited by *C. difficile* (sorbitol [97,98], mannitol [97,98], trehalose [29,32], and
595 succinate [56,97]) (**Fig. 5a**). In monoculture, all gut species consumed glucose, but sorbitol
596 was consumed by CS and CH, and mannitol was consumed by CH (**Fig. S19a**).

597 To evaluate whether species richness in a community also influences the degree
598 of variability, we randomly assembled communities with different species richness. The
599 Euclidean distances of species relative abundance between all pairs of replicates
600 increased over time more consistently in the media with multiple *C. difficile*-preferred
601 carbohydrates. In media containing only glucose, the Euclidean distance displayed non-
602 monotonic trends over time (**Fig. 5b**). Overall, the Euclidean distances were higher in
603 communities with higher species richness in both media types, and in the media
604 containing only glucose than in media with multiple *C. difficile*-preferred carbohydrates.
605 Although *C. difficile* abundance was lower in the glucose-only media [55], the variability in
606 its abundance was higher than in multiple preferred carbohydrates (**Fig. 5c, S19b**). This
607 highlights a potential trade-off between high variability versus strong inhibition of *C.
608 difficile* due to variations in the nutrient landscape.

609 Variability in propagule pressure of *C. difficile* (i.e. initial abundance in the
610 community at the beginning of each passage) could contribute to the variability in
611 abundance across repetitive regrowth cycles [14]. To determine how nutrient environment
612 shapes the sensitivity to variation in propagule pressure, we characterized community
613 assembly in the glucose-only media versus multiple *C. difficile*-preferred carbohydrates
614 media (**Fig. S19c**). In the glucose-only media, *C. difficile* growth displays a larger change
615 as a function of its initial amount in low to medium-richness communities compared to the
616 multiple *C. difficile*-preferred carbohydrates media, i.e. more sensitive to propagule
617 pressure (**Fig. S19d**). Thus, the sensitivity to initial abundance in different nutrient
618 environments can provide insights into the observed variability in community dynamics.

619

DISCUSSION

621 The community-acquired incidence of CDI continues to rise despite the expanding
622 treatment options including FMT and emerging defined bacterial therapeutics [99-101]. *C.
623 difficile* can colonize individuals for yearlong timescales [6,8,10,102] and act as a reservoir for
624 *C. difficile,* increasing the chance of infection in the host [16] and other individuals via
625 transmission [8,19-21]. Identifying strategies that reduce *C. difficile*'s ability to persist in the
626 human gut could potentially reduce the prevalence and severity of CDI. Human gut
627 microbiota interactions are major variables influencing colonization ability. However, we
628 lack an understanding of the molecular and ecological mechanisms shaping *C. difficile*
629 growth in communities over long timescales. We exploited high-throughput *in vitro*

630 experiments combined with dynamic ecological modeling to understand the role of
631 community context on the ability of *C. difficile* to coexist with diverse human gut bacteria
632 and elucidate factors shaping variability in its growth over hundreds of generations. We
633 identified key species that display stable coexistence or unstable dynamics with *C. difficile*,
634 consistent with the quantitative effects of their inferred inter-species interactions on
635 community dynamics. Our findings yield insights into the ability of *C. difficile* to persist in
636 different gut communities, which could aid in devising strategies to reduce its persistence.
637 Importantly, we found that prolonged co-culture of *C. difficile* with PV could lead to *C.*
638 *difficile* evolutionary adaptation that reduces its virulence through metabolic alterations.
639 This opens up a new avenue for *C. difficile* interventions where bacterial therapeutics or
640 diets could be designed to steer *C. difficile* evolutionary adaptations towards reduced
641 colonization ability and attenuated virulence.

642 The variability of *C. difficile* across individuals could influence transmission and
643 disease outcomes. For example, higher variability generates higher uncertainty of *C.*
644 *difficile* growth or toxin production and could reduce the predictability and efficacy of
645 treatments for CDI. We demonstrated that certain pairs of species have more unstable
646 dynamics across different community contexts and nutrient environments (**Fig. 1f, S5h-**
647 **j**), which leads to higher variability in growth. Further, nutrient environments and the
648 number of species in the community can also influence variability in *C. difficile* growth
649 over long timescales. Using a library of isolates from soil samples and *Caenorhabditis*
650 *elegans* intestine, a previous study [103] demonstrated that increasing the number of
651 species in the community or nutrient concentrations [104,105] reduced the stability of
652 community dynamics, shifting the system from stable coexistence to persistent
653 fluctuations. In this study, we observed that communities with higher species richness
654 displayed higher variability in abundances over long timescales (**Fig. 5**). While fixing the
655 total amount of carbon, there was higher variability in community composition and *C.*
656 *difficile* abundance in an environment containing a single accessible resource as opposed
657 to multiple distinct resources. An environment with a single accessible resource may
658 enhance the strength of resource competition and/or production of toxic metabolic
659 byproducts. While *C. difficile*'s abundance was reduced in this environment, its variability
660 was enhanced, highlighting a potential trade-off.

661 The human gut microbiome is dominated by *Bacteroides* species such as PV [75-78]
662 that stably engraft for long timescales [106-108]. PV has been highlighted as a potential
663 candidate for live bacterial therapeutics to treat recurrent CDI (rCDI) due to its high
664 engraftment efficiency [108]. Supporting this notion, PV was a dominant member in a 7-
665 member bacterial community in germ-free mice (~50% fraction across all conditions) and
666 maintained a high relative abundance for up to 2 weeks even after the mice were
667 challenged with *C. difficile* (**Fig. S17**). Understanding how highly abundant and stable
668 members of the human gut microbiome coexist and interact with *C. difficile* over the long
669 term could have important therapeutic implications. Our results demonstrated that
670 decreasing the concentration of carbohydrates shifted PV and *C. difficile* community
671 dynamics from competitive exclusion to coexistence over 341 generations (**Fig. 2, S5e-**

672 **f**). Using exo-metabolomic profiling, we revealed that this coexistence can be explained
673 by a high degree of metabolite cross-feeding from PV to *C. difficile*, including major amino
674 acids that fuel *C. difficile*'s Stickland metabolism. This cross-feeding of amino acids from
675 *Bacteroides* to *Clostridium* species has been previously reported [82], and there are other
676 *in vitro* and *in silico* evidence of amino acids cross-feeding among gut microbes [82,109]. Our
677 results suggest that cross-feeding was not present in the presence of high carbohydrate
678 concentrations, consistent with a previous study showing that high concentrations of
679 acetate suppress the release of amino acids by *Bacteroides* species [83]. Notably, a
680 moderate reduction in the concentrations of key resources could massively alter the
681 interactions between PV and *C. difficile*. This implies that diet could be precisely
682 manipulated to alter interactions between gut microbes and *C. difficile* and influence the
683 evolutionary trajectories of *C. difficile*.

684   Persistent colonization enables *C. difficile* to adapt to changing environments
685 within the human gut. Evolutionary adaptations of *C. difficile* could impact the host through
686 alterations in metabolism and virulence [29-32]. Our current knowledge of *C. difficile*'s
687 evolution is largely based on retrospective sequencing-based analyses [110] and genome
688 comparisons to reveal genetic changes predicted to alter key phenotypes [29,31,32,111-113].
689 We lack an understanding of the role of human gut microbiota inter-species interactions
690 on *C. difficile* evolutionary adaptations. Our study demonstrated that prolonged
691 coexistence between *C. difficile* and PV yielded evolutionary adaptations in *C. difficile*
692 that shifted its metabolism from consuming proline to glucose and altered its fitness under
693 different concentrations of resources (**Fig. 3, S13-14, Table S4**). These metabolic
694 changes enhanced its ability to coexist with PV (**Fig. S9b**). Although a previous study
695 showed that *C. difficile* strains with large genotypic variations have minimal differences in
696 inter-species interactions with human gut bacteria [55], here we demonstrate that two
697 single-point mutations in *C. difficile* metabolic genes could substantially alter the
698 interaction networks with human gut microbiota (**Fig. 4a-d**). This implies that although
699 human gut microbiota inter-species interactions with *C. difficile* are generally robust to
700 genotypic variations, a small number of mutations in key genes could yield large changes
701 in the interaction network.

702   An important question is whether this metabolic adaptation of *C. difficile* alters
703 disease severity or propensity for CDI. Proline metabolism of *C. difficile* has been shown
704 to affect toxin production [79] and colonization of the murine gut [80]. Indeed, our evolved *C.*
705 *difficile* strain displayed a substantial reduction in toxin production and colonization ability,
706 thus ameliorating disease severity in the murine gut compared to the ancestral *C. difficile*
707 strain (**Fig. 4e-i**). Deletion of *prdB* in *C. difficile,* an essential enzyme in the proline
708 Stickland fermentation pathway [79], reduced colonization and toxin production in the
709 murine gut [80]. This is consistent with the reduced disease severity observed in mice
710 colonized with the evolved *C. difficile* strain which has evolved to use less proline. These
711 results demonstrate that proline utilization plays a critical role in the colonization and
712 infection process. Our study highlights how two-point mutations in the *C. difficile* genome
713 from evolutionary adaptation can substantially alter virulence and colonization ability. This

714 implies that *C. difficile*'s pathogenic potential displays fragility to mutations in specific
715 genes. *C. difficile* clinical isolates have displayed variable effects on mice [114] and avirulent
716 strains have been shown to protect against CDI by outcompeting the virulent *C. difficile*
717 strains [115]. As opposed to eliminating *C. difficile* from the gut, future studies could
718 investigate interventions that steer *C. difficile* metabolic states and suppress its virulence
719 (e.g. shifting away from proline utilization) while also promoting colonization and fitness
720 in the gut, thus protecting against virulent *C. difficile* strains.

721

Materials and Methods

Strain, media, and growth conditions

724 The strains used in this work were obtained from the sources listed in **Table S1**. The non-
725 toxigenic *C. difficile* isolate MS001 was obtained from a previous study [55]. Single-use
726 glycerol stocks were prepared as described previously [51]. The media used in this work
727 are anaerobic basal broth (ABB, Oxoid) for growing starter cultures, and in-house Defined
728 Media (DM) formulated based on previous study [51] (recipe in **Table S2**).

729 For all experiments, cells were cultured in an anaerobic chamber (Coy Lab
730 products) with an atmosphere of $2.0 \pm 0.5\%$ H_2, $15 \pm 1\%$ CO_2, and balance N_2 at 37 C.
731 Starter cultures were inoculated by adding 200 µl of a single-use 25% glycerol stock to 5
732 ml of anaerobic basal broth media (ABB) and grown at 37 C without shaking.

733

Long-term growth experiments

735 Starter cultures of *C. difficile* and gut commensal bacteria were prepared. For
736 experiments in **Fig. 1**, the media used are DM, DM with 75% less carbohydrate
737 concentration, and DM with 100% higher amino acid concentration. For experiments in
738 **Fig. 5**, the media used are DM containing only 5 g/L glucose as a sole carbohydrate
739 source, and DM containing 1 g/L glucose, 1 g/L sorbitol, 1 g/L mannitol, 1 g/L trehalose,
740 and 1 g/L succinate as carbohydrate sources.

741 The cell pellets from starter cultures were collected by centrifugation at 3,000 x g
742 for 5 min, and then washed with experimental media. The washed cell pellets were
743 resuspended into the experimental media to a final OD_{600} of approximately 0.1. To
744 assemble communities, the monocultures of *C. difficile* and each gut species were mixed
745 in equal proportions based on OD_{600} and inoculated into a 2 mL 96-deep-well plate (Nest
746 Scientific) containing experimental media to an initial OD_{600} of 0.01. For instance, the
747 OD_{600} of each species in two-member and 6-member communities are 0.01/2=0.005 and
748 0.01/6=0.00167 respectively. These plates were covered with gas permeable seal
749 (Breathe-Easy® sealing membrane) and incubated at 37 ºC anaerobically. After every 24
750 hours, OD_{600} was measured with a Tecan F200, and the cells were passaged with 40X
751 dilution to new 96-deep-well plates containing experimental media. The monocultures of

752 individual species in the community were also inoculated and passaged as a control and
753 to monitor for changes in carrying capacity. Every 7 days, aliquots of the cultures were
754 preserved as glycerol stocks and cell pellets were collected for DNA extraction, PCR
755 amplification, and NGS sequencing. Depending on the experiment, the communities were
756 maintained for 35 to 64 passages. We calculated the number of generations per passage
757 as the $\log_2$ of the dilution factor [116]. Thus, we estimate that the communities were
758 maintained for up to 341 generations, which is long enough for adaptation to occur based
759 on previous studies [41,42].

760

Isolation of *C. difficile* strains from communities

762 Communities from the evolution experiments were preserved as glycerol stocks. Aliquots
763 from the glycerol stock were streaked into *C. difficile* selective plates to isolate single
764 colonies, the plates were incubated at 37°C for 24 h, and the *C. difficile* strain was grown
765 in a liquid culture from a single colony.

766   *C. difficile* selective plates were prepared by autoclaving *C. difficile* agar (Oxoid
767 CM0601) and adding horse blood (Lampire 7233401, 70 mL/1L media), norfloxacin
768 (Santa Cruz 215586, 120 µg/mL), moxalactam (Santa Cruz 250419, 320 µg/mL), and
769 erythromycin (Santa Cruz 204742, 100 µg/mL) after the media cooled to 55°C.

770

Fluorescence microscopy of *C. difficile*

772 Starter cultures of the evolved and ancestral *C. difficile* strain were prepared. The cell
773 pellets from starter cultures were collected by centrifugation at 3,000 x g for 10 min, and
774 then washed with DM. The washed cell pellets were resuspended into DM to a final OD_{600}
775 of approximately 0.1. These cultures were inoculated into new culture tubes containing
776 DM to an initial OD_{600} of 0.01 by adding 500 µl of washed starter cultures to 4.5 mL media.
777 After 6 h and 24 h of growth, 100 µl aliquots were taken, stained with SYBR Green dye,
778 and viewed with a microscope (Nikon Eclipse Ti-E inverted microscope) at 20× dry
779 objective with appropriate filter sets. Images were captured with Photometrics CoolSNAP
780 Dyno CCD camera and associated software (NIS-Elements Ver. 4.51.00).

781

Logistic growth model

783 The logistic growth model was used to describe population growth dynamics in
784 monoculture experiments. The logistic growth model for species i takes the following form:

785
$$\frac{dx_i}{dt} = x_i \left(r_i - \frac{r_i}{K_i} x_i \right)$$

786 where x_i is the absolute abundance of species i, parameter r_i is its maximum growth rate,
787 and K_i is its carrying capacity. We cut time points where the OD_{600} drops below > 10% to

788 exclude the death phase. Thus, the steady-state solution of the model is the carrying
789 capacity (K_i) (i.e. the value of x_i when $\frac{dx_i}{dt}$ equals 0). We also excluded data points less
790 than 120% of the initial OD_{600} (OD_{600} at t=0) to exclude the lag phase which is not captured
791 in the logistic model. A custom MATLAB script is used to estimate the parameters $\theta_i =$
792 $[r_i, K_i]$ in the logistic growth model. For each species *i*, the model is fitted to experimental
793 data with L2 regularization. Specifically, given a series of *m* experimental OD_{600}
794 measurements, $\boldsymbol{x_i} = [x_{i,1}, \cdots, x_{i,m}]$, and a series of OD_{600} simulated using parameter θ_i at
795 the same time intervals, $\hat{\boldsymbol{x}}_i(\boldsymbol{\theta_i}) = [\hat{x}_{i,1}(\theta_i), \cdots, \hat{x}_{i,m}(\theta_i)]$, the optimization scheme
796 minimizes the cost function:

797
$$C(\theta_i) = |\widehat{X_i}(\theta_i) - X_i|_2 + \lambda|\theta_i|_2,$$

798 where λ is the L2 regularization parameter and $|\cdot|_2$ indicates vector 2-norm. To find a
799 suitable regularization parameter λ, we took λ values from the set $(10^{-3}, 3 \times$
800 $10^{-3}, 10^{-2}, 3 \times 10^{-2}, 0.1, 0.3, 1, 3, 10)$. Based on the cost for each species as a function of
801 λ, we picked regularization parameter λ = 0.03. Solutions to the logistic growth model
802 were obtained using the ode15s solver and the optimization problem was solved using
803 FMINCON in MATLAB (R2022a).

804

Bacterial genome DNA extraction and next-generation sequencing

806 All the genomic DNA (gDNA) extraction and next-generation sequencing sample
807 preparation were performed as described previously [51,55]. Bacterial gDNA extractions
808 were carried out using a modified version of the Qiagen DNeasy Blood and Tissue Kit
809 protocol in 96-well plates. Briefly, cell pellets were resuspended in 180-µl enzymatic lysis
810 buffer containing 20 mg/ml lysozyme (Sigma-Aldrich), 20 mM Tris–HCl pH 8 (Invitrogen),
811 2 mM EDTA (Sigma-Aldrich), and 1.2% Triton X-100 (Sigma-Aldrich), and then incubated
812 at 37°C at 600 RPM for 30 min. Samples were treated with 25 µL 20 mg/ml Proteinase K
813 (VWR) and 200 µL buffer AL (Qiagen), mixed by pipette, and then incubated at 56°C at
814 600 RPM for 30 min. Samples were treated with 200 µL 200 proof ethanol (Koptec), mixed
815 by pipette, and transferred to 96-well nucleic acid binding plates (Pall). After washing with
816 500 µL buffer AW1 and AW2 (Qiagen), a vacuum was applied for 10 min to dry excess
817 ethanol. Genomic DNA was eluted with 110 µL buffer AE (Qiagen) preheated to 56°C and
818 then stored at −20°C.

819 Genomic DNA concentrations were measured using the Quant-iT™ dsDNA Assay
820 Kit (Invitrogen) with a 6-point DNA standard curve (0, 0.5, 1, 2, 4, 6 ng/µL biotium). 1 µL
821 of samples and 5 µL of standards were diluted into 95 µL of 1× SYBR green (Invitrogen)
822 in TE buffer and mixed by pipette. Fluorescence was measured with an
823 excitation/emission of 485/535 nm (Tecan Spark). Genomic DNA was then normalized to
824 2 ng/µL by diluting in molecular grade water (VWR International) using a Tecan Evo Liquid
825 Handling Robot.

826   Dual-indexed primers for multiplexed amplicon sequencing of the V3-V4 region of
827   the 16S rRNA gene were designed as described previously [51,60]. PCR was performed
828   using the normalized gDNA as template and Phusion High-Fidelity DNA Polymerase
829   (Thermo Fisher) for 25 cycles with 0.05 µM of each primer. Samples were pooled by plate,
830   purified using the DNA Clean & Concentrator™-5 kit (Zymo) and eluted in water,
831   quantified by NanoDrop, and combined in equal proportions into a library. The library was
832   quantified using Qubit 1× HS Assay (Invitrogen), diluted to 4.2 nM, and loaded at 10 pM
833   onto Illumina MiSeq platform for 300-bp paired-end sequencing using MiSeq Reagent Kit
834   v2 (500-cycle), or loaded at 21 pM using MiSeq Reagent Kit v3 (600-cycle) depending on
835   the desired sequencing reads.

836

Next-generation sequencing data analysis to determine community composition

838   Sequencing data were analyzed as described previously [55,60]. Briefly, reads were
839   demultiplexed with Basespace FastQ Generation, and the FastQ files were analyzed
840   using custom Python scripts. Paired reads were merged using PEAR (Paired-End reAd
841   mergeR) v0.9.0 [117]. A reference database containing 16S V3-V4 region of each species
842   in the study was created by assembling consensus sequence based on sequencing
843   results of each monospecies. Reads were mapped to the reference database using the
844   mothur v1.40.5 command classify.seqs using the Wang method with bootstrap cutoff
845   value of 60% [118,119]. Relative abundance was calculated by dividing the read counts
846   mapped to each organism by the total reads in the sample. Absolute abundance was
847   calculated by multiplying the relative abundance of an organism by the OD_{600} of the
848   sample as previously described [14,60]. Samples were excluded from further analysis if > 1%
849   of the reads were assigned to a species not expected to be in the community (indicating
850   contamination).

851

generalized Lotka-Volterra models for fitting non-passaging data

853   The generalized Lotka-Volterra (gLV) model is a set of coupled ordinary differential
854   equations that describe the growth of interacting species over time,

855
$$\frac{dx_i}{dt} = x_i \left(r_i + \sum_{j=1}^{n_s} a_{ij} x_j \right)$$

856   where x_i is the abundance of species i and n_s is the total number of species. Model
857   parameters that need to be estimated from data include the species growth rate, denoted
858   as r_i, and coefficients that determine how species j affects the growth of species i,
859   denoted as a_{ij}. The data used for parameter estimation is the growth of species over time
860   under different inoculation conditions. For monoculture growth data, we use OD_{600}
861   measurements only, whereas for community data, this was obtained by multiplying the

862 relative abundance obtained from 16S sequencing by the total OD_{600}. The dataset used
863 to fit the gLV model is DATASET002 (**Table S3**).

864   A prior over the parameter distribution is set so that growth rates have a mean of
865 0.3, self-interaction terms have a mean of -1, and inter-species interaction terms have a
866 mean of -0.1. Given a dataset of measured species abundances over time after
867 inoculating different combinations of species, the model parameters are determined by
868 minimizing a cost function given by a weighted squared difference between model-
869 predicted species abundances and measured abundances and a penalty for deviations
870 from the prior mean. Using the fitted parameter estimates, the covariance of the posterior
871 parameter distribution is approximated as the inverse of the Hessian (matrix of second
872 derivatives) of the cost function with respect to the model parameters. The Expectation-
873 Maximization (EM) algorithm is used to optimize the precision of the prior parameter
874 distribution and the precision of the noise distribution, which collectively determine the
875 degree to which estimated parameters are penalized for deviations from the prior mean
876 [120]. In other words, the precision of the prior and noise are hyperparameters that
877 determine the degree of regularization. To evaluate model prediction performance on
878 held-out data, we performed 10-fold cross validation where the degree of regularization
879 was optimized using the EM algorithm and only community samples were subjected to
880 testing (i.e. monoculture data was reserved only for model training). See **Supplementary**
881 **Text** for a more detailed description of parameter estimation and the EM algorithm.

882

883 **Generalized Lotka-Volterra models for fitting long-term passaging data**

884 A general Lotka-Volterra (gLV) model with elastic net regularization was used to simulate
885 long-term growth experiments with passaging (repetitive regrowth cycles):

886
$$L = \sum_{k=1}^{K}\sum_{j=1}^{M}\sum_{i=1}^{N}(y_{ijk} - \hat{y}_{ijk}) + \lambda_1\left(\lambda_2\sum_{i=1}^{Z}p_i^2 + (1-\lambda_2)\sum_{i=1}^{Z}|p_i|\right)$$

887
$$A = \begin{bmatrix} p_1 & \cdots & p_{N\times(N-1)} \\ \vdots & \ddots & \vdots \\ p_N & \cdots & p_{N\times N} \end{bmatrix}, \qquad A_{ii} \leq 0$$

888
$$\mu^T = [p_{N\times N+1} \quad \cdots \quad p_{N\times(N+1)}], \qquad \mu \geq 0$$

889
$$\frac{dY}{dt} = Y \odot (AY + \mu), \qquad \text{where } \odot \text{ is elementwise multiplication}$$

890
$$Y^T = [y_1 \quad \cdots \quad y_N]$$

891 where $\hat{y}$ is the predicted output, y is the observed output or species normalized optical
892 density (OD), K is the number of passages, M is the number of averaged experimental
893 samples, N is the number of species, $\lambda_1 = 10^{-6}$ is the overall elastic net regularization
894 parameter, $\lambda_2 = 0.5$ is the parameter weighing between Ridge and Lasso regularization,
895 p_i are the general Lotka-Volterra (gLV) parameters, A is the inferred gLV interaction
896 matrix, and μ are the inferred gLV growth rates. To obtain the predictions, we integrated

897   Y over a time span $[0, t_f]$, where $t_f = 24$, using a fixed-step Euler's method for simplicity
898   and applied a 40-fold dilution to the end time point of each integration T times for T
899   passages. The loss was optimized using a global constrained optimization algorithm (Low
900   Discrepancy Sequence Multi-Level Single-Linkage) with a population of 32 samples and
901   a local optimizer Sbplx, a more robust Nelder-Mead method [121-124]. The diagonals of
902   matrix A are constrained to be negative, and μ was constrained to be nonnegative. We
903   fitted 64 models over the entire experimental dataset, and unstable models were
904   discarded to obtain final parameter estimates, for which distribution is assumed Gaussian.
905   The gradient-free optimization method and Euler's method were chosen in favor of
906   gradient-based optimization and adaptive higher-order ordinary differential equation
907   solvers to handle gLV model instability due to long integration times. The dataset used to
908   fit the gLV model is DATASET001 (**Table S3**).

909

Whole-genome sequencing and variant calling

911   We subjected six strains for whole-genome sequencing: Ancestral *C. difficile* DSM 27147
912   and ancestral *P. vulgatus* ATCC 8482 strain, *C. difficile* and PV strain that were passaged
913   alone in the media with reduced carbohydrates concentration, *and C. difficile* and PV
914   strain isolated from CD-PV co-culture after 64 passages in the media with reduced
915   carbohydrates concentration. Cultures were streaked into *C. difficile* selective agar plate
916   (for isolating *C. difficile*) or ABB agar plate (for isolating PV) to isolate single colonies.
917   Although ABB is not selective for PV, its proportion is much higher than *C. difficile* in the
918   CD-PV co-culture and thus has a much higher number of colonies in the ABB agar plate.
919   For all conditions, one colony was isolated, grown to OD_{600} of 0.3, and subjected to whole-
920   genome sequencing. Besides the six strains, we also subjected the whole CD-PV
921   population (all 3 biological replicates) after 35, 49, and 64 passages in the media with
922   reduced carbohydrate concentration to whole-genome sequencing.

923   The cultures were centrifuged to obtain the cell pellets. Genomic DNA was
924   extracted using Qiagen DNeasy Blood and Tissue Kit according to the manufacturer's
925   protocol. The harvested DNA was detected by the agarose gel electrophoresis and
926   quantified by a Qubit fluorometer. The genomic DNA was sent to SeqCenter (Pittsburgh,
927   PA, USA) for paired-ends Illumina sequencing. Sample libraries were prepared using the
928   Illumina DNA Prep kit and IDT 10 bp UDI indices, and sequenced on an Illumina NextSeq
929   2000, producing 2 x 151 bp reads. Demultiplexing, quality control, and adapter trimming
930   were performed with bcl-convert (v3.9.3) Illumina software.

931   To identify mutations in the six strains, we performed variant calling analysis using
932   BreSeq version 0.38.1 [125] with default settings using *C. difficile* R20291 reference genome
933   (GenBank ID: FN545816.1) or *P. vulgatus* ATCC 8482 reference genome, and performed
934   a genomic comparison between the ancestral strain and strains after passaging both in
935   monoculture and co-culture conditions. We only detected two non-synonymous single-
936   point mutations in *gene 206* (G533W) and in *prdR* (A341V) for *C. difficile* from the CD-PV

937 pair, and no mutations in *C. difficile* that was passaged alone, PV that was passaged
938 alone, or PV from CD-PV pair. To identify lower abundance mutations in the CD-PV
939 population, we performed variant calling analysis using Snippy V4.6.0 [126]. To estimate the
940 proportion of mutants in the population, we used the ratio of the number of alternate reads
941 (reads of the mutation) to the total number of reads at the locus (number of alternate
942 reads + number of reference reads) extracted from Snippy vcf result files.

943

Sanger sequencing of the *prdR* gene

945 To check the presence of the *prdR* A341V mutation in other biological replicates of CD-
946 PV co-culture and other pairwise communities, we performed Sanger sequencing on *C.*
947 *difficile* isolated from two other biological replicates of the CD-PV pair after 64 passages,
948 three biological replicates of the CD-BU pair after 64 passages, two biological replicates
949 of the CD-CA pair after 42 passages, one biological replicate of the CD-DP pair after 49
950 passages, one biological replicate of the CD-DP pair after 64 passages, and two
951 biological replicates of the CD-EL pair after 64 passages (one colony each).

952 Aliquots from the glycerol stock of communities at the end of the passaging
953 experiments were streaked into *C. difficile* selective plates to isolate single colonies. The
954 *C. difficile* strains were grown from a single colony to OD_{600} of 0.3. The cultures were
955 centrifuged to obtain the cell pellets. Genomic DNA was extracted using Qiagen DNeasy
956 Blood and Tissue Kit according to the manufacturer's protocol.

957 PCR was performed using the gDNA as a template (2 ng/μL) and Phusion High-
958 Fidelity DNA Polymerase (Thermo Fisher) for 25 cycles with 0.2 μM of each primer. The
959 primers were designed to amplify 526 bp of the *prdR* gene targeting the mutated region
960 (A341V). The primer sequence is *F*: CAGAAGCTAAGATATTAGCTCTTGAA and *R*:
961 ATTGGTAGCTGATATTATTCTAGGA. The amplified PCR product was subjected to
962 Sanger Sequencing (Functional Biosciences).

963

Transcriptomic profiling

965 Ancestral *C. difficile* monoculture, evolved *C. difficile* monoculture, CD ancestral + PV
966 coculture, and CD evolved + PV coculture conditions were inoculated from starter cultures
967 into individual culture tubes containing DM. For monoculture conditions, *C. difficile* was
968 inoculated to an OD_{600} of 0.01. For cocultures, *C. difficile* and PV were inoculated to an
969 equal ratio (OD_{600} of 0.005 each). The cultures were incubated anaerobically at 37°C with
970 no shaking for ~6 h until the culture reached the exponential phase (OD_{600} ~0.2). 1000
971 μL of the culture was taken for OD_{600} measurement and total DNA extraction for next-
972 generation sequencing, and 2000 μL of the culture was taken for total RNA extraction for
973 transcriptomics. 4000 μL of RNAprotect (Qiagen) was added to 2000 μL of culture and
974 incubated for 5 min at room temperature. Cultures were then centrifuged at room
975 temperature for 10 min at 3000 g and the supernatant was carefully removed. Cell pellets

976   were immediately subjected to RNA extraction using acidic phenol bead-beating method.
977   Pellets were resuspended in 500 µL 2× Buffer B (200 mM sodium chloride, 20 mM
978   ethylenediaminetetraacetic acid) and transferred to 2 mL microcentrifuge tubes
979   containing 500 µL Phenol:Chloroform:IAA (125:24:1, pH 4.5) and 210 µL 20% sodium
980   dodecyl sulfate and were bead-beated with acid washed beads (Sigma G1277) for 3 min.
981   All solutions used for RNA extraction were RNAse-free. Samples were centrifuged at 4°C
982   for 5 min at 7,200 g, and 600 µL of the upper aqueous phase was added to 60 µL 3 M
983   sodium acetate and 660 µL cold isopropanol and chilled on ice for 5 min before freezing
984   for 5 min at −80°C. Samples were centrifuged at 4°C for 15 min at 18,200 g, the
985   supernatant was decanted, and the pellet was washed with cold 100% ethanol. The
986   pellets were dried in a biosafety cabinet for 15 min and then resuspended in 100 µL
987   RNAse-free water. Samples were purified using RNeasy Mini Kit (Qiagen) and genomic
988   DNA was removed using RNAse-Free DNase Set (Qiagen). Two replicates of each
989   condition were sent to Novogene Corporation Inc (Sacramaneto, CA, United States of
990   America) for rRNA depletion, cDNA library preparation, and sequencing on Illumina
991   NovaSeq. Data was de-multiplexed using Illumina's bcl2fastq 2.17 software, where one
992   mismatch was allowed for index sequence identification.

993   The compressed FASTQ files were quality-checked using the FastQC tool v0.12.1
994   [127]. The BBDuk, BBSplit, and BBMap tools from BBTools suite (v38.42) [128] were used to
995   trim adapters, deplete rRNA, and map the remaining mRNA reads to the reference
996   genomes. For monoculture or cocultures containing *C. difficile*, the reference genome
997   was obtained from GenBank (FN545816.1). The feature-Counts package v1.6.4 [129] from
998   the SubRead suite was used to map reads to features on the genome and quantify raw
999   counts for each transcript. Reads per kilobase million (RPKM) values were computed
1000   using a custom Python script to see the agreement of gene expression between biological
1001   replicates. The gene expression (represented by RPKM values) shows a good correlation
1002   between biological replicates (Pearson's R=0.97-0.98, P<10E-05) (**Fig. S11b**). The
1003   DESeq2 Bioconductor library v4.0.3 [130] was used in R v4.0.4 to quantify differential gene
1004   expression using a negative binomial generalized linear models with apeglm shrinkage
1005   estimator [131]. When calculating RPKM of *C. difficile* genes in the CD-PV cocultures, the
1006   "reads mapped" in the denominator was the number of reads mapped to the *C. difficile*
1007   genome. Similarly, when quantifying differential gene expression for *C. difficile* genes in
1008   the CD-PV cocultures, only reads mapped to the *C. difficile* genome were provided to
1009   DeSeq2. We define differentially expressed genes (DEGs) as those with >2-fold change
1010   and a *p*-value less than 0.05.

1011

C. difficile toxin measurements using ELISA

1013   Toxin (both TcdA and TcdB) concentrations were determined in the ancestral and evolved
1014   *C. difficile* strains by comparison to a standard curve using ELISA (tgcBiomics, Germany).
1015   The blank media used to grow the cultures were also included in the assay to measure
1016   any background noise. All the samples subjected to toxin measurements in this study

1017 were processed in parallel at the same time using the same batch of ELISA kits to
1018 minimize batch-to-batch variations and ensure comparable results.

1019

Exo-metabolomic profiling

1021 Starter cultures of *C. difficile* and gut bacteria were prepared. The cell pellets from starter
1022 cultures were collected by centrifugation at 3,000 x g for 5 min, and then washed with
1023 either DM or DM with reduced carbohydrate concentration. The washed cell pellets were
1024 resuspended into either DM or DM with reduced carbohydrate concentration to a final
1025 OD_{600} of approximately 0.1. For monocultures, bacteria were inoculated to an OD_{600} of
1026 0.01 in media containing either DM or DM with reduced carbohydrate concentration. For
1027 co-cultures, *C. difficile* and PV were inoculated to an equal ratio (OD_{600} of 0.005 each) in
1028 media containing either DM or DM with reduced carbohydrate concentration. The cultures
1029 were incubated at 37 ºC anaerobically. Three biological replicates were performed for
1030 each sample. At specific time points (6, 12, or 24 hours), the cultures were centrifuged at
1031 3,000 x g for 10 min, and the supernatants were filter sterilized.

1032 For metabolite extraction, 25 µL of each sterilized supernatants sample were
1033 pipetted into a microcentrifuge tube. The extraction solvent consisted of 1:1
1034 methanol:ethanol containing 22 µM D4-succinate (Sigma 293075). 112.5 µL of the
1035 extraction solvent was added to each sample, followed by a 10 min incubation on ice.
1036 Then, 87.5 µL of molecular biology-grade water was added to the extraction tube,
1037 followed by another 10 min incubation on ice. The samples were centrifuged at 16,000 x
1038 g for 10 min at 4°C, and the supernatant (190 µL) was transferred to a Captiva cartridge
1039 (Agilent 5190-1002, 1mL). The sample was allowed to flow through under vacuum,
1040 followed by two elutions with 250 µL of 2:1:1 water:methanol:ethanol. Both the
1041 flowthrough and the elutions were collected in one tube and evaporated under vacuum at
1042 45°C for 2 h. The dried metabolite pellet was stored at -80°C until it was resuspended in
1043 70:20:10 acetonitrile:water:methanol (100 µL) prior to LC/MS analysis.

1044 Extracts were separated on an Agilent 1290 Infinity II Bio LC System using an
1045 InfinityLab Poroshell 120 HILIC-Z column (Agilent 683775-924, 2.7 µm, 2.1 x 150 mm),
1046 maintained at 15°C. The chromatography gradient included mobile phase A containing
1047 20 mM ammonium acetate in water (pH 9.3) and 5 µM of medronic acid, and mobile phase
1048 B containing acetonitrile. The mobile phase gradient started with 10% mobile phase A
1049 increased to 22% over 8 min, increased to 40% by 12 min, 90% by 15 min, and then held
1050 at 90% until 18 min before re-equilibration at 10% (held until 23 min). The flow rate was
1051 maintained at 0.4 mL/min for most of the run, but increased to 0.5 mL/min from 19.1 min
1052 to 22.1 min. The UHPLC system was connected to an Agilent 6595C QqQ MS dual AJS
1053 ESI mass spectrometer. This method was operated in polarity-switching mode. The gas
1054 temperature was kept at 200°C with flow at 14 L/min. The nebulizer was at 50 PSI, sheath
1055 gas temperature at 375°C, and sheath gas flow at 12 L/min. The VCap voltage was set
1056 at 3000V, iFunnel high pressure RF was set to 150 V, and iFunnel low pressure RF was

1057 set to 60 V in positive mode. In negative mode, the VCap voltage was set to 2500 V, the
1058 iFunnel high pressure RF was set to 60 V, and iFunnel low pressure RF was set to 60 V.
1059 A dMRM inclusion list was used to individually optimize fragmentation parameters. The
1060 injection volume was 1 μL.

1061   Raw data was collected in .d format and checked manually in Agilent MassHunter
1062 Qualitative Analysis. The data was then uploaded to Agilent MassHunter Quantitative
1063 Analysis for quantitation using relative internal standard calculations to calculate analyte
1064 concentrations. After manual inspection and integration, analyte concentration (ng/mL of
1065 reconstituted extract) was exported to .csv files.

1066

HPLC quantification of organic acids

1068 Starter cultures of ancestral *C. difficile*, evolved *C. difficile*, and PV were prepared. The
1069 cell pellets from starter cultures were collected by centrifugation at 3,000 x g for 5 min,
1070 and then washed with DM or DM with reduced concentration of carbohydrates. The
1071 washed cell pellets were resuspended into the respective media to a final OD_{600} of
1072 approximately 0.1, inoculated into a 5 mL culture tubes to an initial OD_{600} of 0.01, and
1073 incubated at 37 ºC anaerobically. For co-cultures, *C. difficile* and PV were inoculated to
1074 an equal ratio (OD_{600} of 0.005 each). Three biological replicates were performed for each
1075 sample.

1076   After 24 hours, the cultures were centrifuged at 3,000 x g for 10 min, and the
1077 supernatants were filter sterilized. Then, 2 μL of H_2SO_4 was added to the supernatant
1078 samples to precipitate any components that might be incompatible with the running buffer.
1079 The samples were then centrifuged at 3,000 x g for 10 min and then 150 μL of each
1080 sample was filtered through a 0.2 μm filter using a vacuum manifold before transferring
1081 70 μL of each sample to an HPLC vial. HPLC analysis was performed using a Shimadzu
1082 HPLC system equipped with a SPD-20AV UV detector (210 nm). Compounds were
1083 separated on a 250 × 4.6 mm Rezex© ROA-Organic acid LC column (Phenomenex
1084 Torrance, CA) run with a flow rate of 0.2 mL min^{-1} and at a column temperature of 50 °C.
1085 The samples were held at 4 °C prior to injection. Separation was isocratic with a mobile
1086 phase of HPLC grade water acidified with 0.015 N H_2SO_4 (415 μL L^{-1}). At least two
1087 standard sets were run along with each sample set. Standards were 100, 20, 4, and
1088 0.8 mM concentrations of butyrate, succinate, lactate, and acetate, respectively. The
1089 injection volume for both sample and standard was 25 μL. The resultant data was
1090 analyzed using the Shimadzu LabSolutions software package.

1091

Hill function fitting

1093 The sensitivity of *C. difficile* growth to proline or glucose concentration was quantified by
1094 fitting the data to the Hill equation:

1095
$$\frac{E}{E_{max}} = \frac{[S]^n}{EC_{50}^n + [S]^n}$$

1096 where E is the normalized Area Under the Curve of *C. difficile* growth for 24 h (AUC$_{24h}$),
1097 E_{max} is the maximum normalized AUC$_{24h}$ across all proline/glucose concentrations, $[S]$ is
1098 the proline/glucose concentration, EC_{50} is the proline/glucose concentration that
1099 produces 50% of E_{max} value, and n is a measure of ultrasensitivity. The data were fit
1100 using the curve_fit function of the scipy package optimization module in Python.

1101

Gnotobiotic mouse experiments

1102

1103 All germ-free mouse experiments were performed following protocols approved by the
1104 University of Wisconsin-Madison Animal Care and Use Committee. We used 12-week-
1105 old C57BL/6 gnotobiotic male mice (wild-type) and a regular diet (Chow diet, Purina,
1106 LabDiet 5021). All bacterial strains were grown at 37 ºC anaerobically in Anaerobe Basal
1107 Broth (ABB, Oxoid) to stationary phase. Commensal gut bacteria strains for oral gavage
1108 were mixed in equal proportions based on OD$_{600}$, whereas *C. difficile* strains for oral
1109 gavage were diluted to an OD$_{600}$ corresponding to ~50,000 CFU/mL based on prior
1110 conversion calculation from CFU counting. These cultures were transferred to Hungate
1111 tubes (Chemglass) on ice prior to oral gavage. To verify and ensure similar dosage for
1112 ancestral *C. difficile* and evolved *C. difficile* gavage, aliquots of *C. difficile* cultures were
1113 plated on agar plates to calculate the exact CFU. The CFU for ancestral *C. difficile* strain
1114 was 50,400 CFU/mL, whereas the CFU for evolved *C. difficile* strain was 49,200 CFU/mL.
1115 On day 0, 0.2 mL of commensal gut bacteria (core community) was introduced into the
1116 mice by oral gavage inside a Biological Safety Cabinet (BSC) and the mice were housed
1117 in biocontainment cages (Allentown Inc.) for the duration of the experiment. After 8 days,
1118 0.2 mL of *C. difficile* (~10,000 CFU) was introduced into the mice by oral gavage. Mice
1119 were maintained for a total of two weeks after the first colonization with the core
1120 community (day 0). Groups of mice (4 mice) with the same core community and *C. difficile*
1121 strain were co-housed in a single cage. Mice were weighed and fecal samples were
1122 collected at specific time points after oral gavage for NGS sequencing and CFU counting.
1123 Cecal contents from mice that were dead or sacrificed were collected for NGS sequencing,
1124 CFU counting, and toxin assay.

1125

Genomic DNA extraction from fecal and cecal samples

1126

1127 The DNA extraction for fecal and cecal samples was performed as described previously
1128 with some modifications [132]. Fecal samples (~50 mg) were transferred into solvent-
1129 resistant screw-cap tubes (Sarstedt Inc) with 500 µL 0.1 mm zirconia/silica beads
1130 (BioSpec Products) and one 3.2 mm stainless steel bead (BioSpec Products). The
1131 samples were resuspended in 500 µL of Buffer A (200 mM NaCl (DOT Scientific), 20 mM
1132 EDTA (Sigma) and 200 mM Tris·HCl pH 8.0 (Research Products International)), 210 µL
1133 20% SDS (Alfa Aesar) and 500 µL phenol/chloroform/isoamyl alcohol (Invitrogen). Cells
1134 were lysed by mechanical disruption with a bead-beater (BioSpec Products) for 3 min
1135 twice, while being placed on ice for 1 min in between to prevent overheating. Next, cells

1136 were centrifuged for 7 min at 8,000 x g at 4°C, and the supernatant was transferred to an
1137 Eppendorf tube. We added 60 μL 3M sodium acetate (Sigma) and 600 μL isopropanol
1138 (LabChem) to the supernatant and incubated on ice for 1 h. Next, samples were
1139 centrifuged for 20 min at 18,000 x g at 4°C, and the supernatant was decanted. The
1140 harvested DNA pellets were washed once with 500 μL of 100% ethanol (Koptec), and the
1141 remaining trace ethanol was removed by air drying the samples. Finally, the DNA pellets
1142 were resuspended into 300 μL of AE buffer (Qiagen). The crude DNA extracts were
1143 purified by a Zymo DNA Clean & Concentrator™-5 kit (Zymo Research) prior to PCR
1144 amplification and NGS sequencing.

1145

1146 *C. difficile* **colony-forming unit counting from fecal and cecal samples**

1147 *C. difficile* selective plates were prepared by autoclaving *C. difficile* agar (Oxoid CM0601)
1148 and adding defibrinated horse blood (Lampire 7233401, 70 mL/1L media), norfloxacin
1149 (Santa Cruz 215586, 120 μg/mL), moxalactam (Santa Cruz 250419, 320 μg/mL), and
1150 erythromycin (Santa Cruz 204742, 100 μg/mL) after the media is cooled to ~55°C. Right
1151 after mice fecal or cecal collection, around 1μL of fresh fecal samples were taken using
1152 an inoculating loop and mixed with PBS. The samples were then serially diluted (1:10
1153 dilution) using PBS. Four dilutions of each sample were spotted on *C. difficile* selective
1154 agar plates, with 2 technical replicates per sample. Plates were incubated at 37°C for 48
1155 h at which point colonies were counted in the dilution spot containing between 5 and 100
1156 colonies. The CFU/mL for each sample was calculated as the average of the 2 technical
1157 replicates times the dilution factor. The lower limit of detection for the assay was 20,000
1158 CFU/mL.

1159

Data availability

1161 Whole-genome sequencing data will be deposited to the NCBI database. RNA-seq data
1162 used in this study will be deposited in the NCBI database. Raw DNA sequencing data
1163 and processed sequencing data to determine community composition will be made
1164 available via Zenodo prior to publication. Exo-metabolomics profiling data will be made
1165 available via Zenodo prior to publication or provided as Source Data file.

1166

Code availability

1168 Codes for fitting the logistic growth model, processing sequencing data and fitting the gLV
1169 models will be available through Github prior to publication. The codes are provided to
1170 the reviewers during peer review.

1171

Acknowledgment

Authors contribution

J.E.S. and O.S.V. conceived the study. J.E.S. carried out the experiments. J.T., P.L.K.C., and Y.Q. implemented computational modeling for the logistic growth model and gLV models. J.M., I.J., and J.S. performed LC-MS metabolomics of bacterial supernatants. J.E.S. and O.S.V. analyzed data. J.E.S. and O.S.V. wrote the paper and all authors provided feedback on the manuscript. O.S.V. secured funding.

Competing interests

The authors declare no competing interests.

References

(1)   Cornely, O. A.; Miller, M. A.; Louie, T. J.; Crook, D. W.; Gorbach, S. L. Treatment of first recurrence of Clostridium difficile infection: fidaxomicin versus vancomycin. *Clinical infectious diseases* **2012**, *55*, S154-S161.
(2)   Nakamura, S.; Mikawa, M.; Nakashio, S.; Takabatake, M.; Okado, I.; Yamakawa, K.; Serikawa, T.; Okumura, S.; Nishida, S. Isolation of Clostridium difficile from the feces and the antibody in sera of young and elderly adults. *Microbiology and immunology* **1981**, *25*, 345-351.
(3)   Kobayashi, T. Studies on Clostridium difficile and antimicrobial associated diarrhea or colitis. *The Japanese journal of antibiotics* **1983**, *36*, 464-476.
(4)   George, R. The carrier state: Clostridium difficile. *Journal of Antimicrobial Chemotherapy* **1986**, *18*, 47-58.
(5)   Czepiel, J.; Dróżdż, M.; Pituch, H.; Kuijper, E. J.; Perucki, W.; Mielimonka, A.; Goldman, S.; Wultańska, D.; Garlicki, A.; Biesiada, G. Clostridium difficile infection. *European Journal of Clinical Microbiology & Infectious Diseases* **2019**, *38*, 1211-1221.
(6)   Kato, H.; Kita, H.; Karasawa, T.; Maegawa, T.; Koino, Y.; Takakuwa, H.; Saikai, T.; Kobayashi, K.; Yamagishi, T.; Nakamura, S. Colonisation and transmission of Clostridium difficile in healthy individuals examined by PCR ribotyping and pulsed-field gel electrophoresis. *Journal of medical microbiology* **2001**, *50*, 720-727.
(7)   Viscidi, R.; Willey, S.; Bartlett, J. G. Isolation rates and toxigenic potential of Clostridium difficile isolates from various patient populations. *Gastroenterology* **1981**, *81*, 5-9.
(8)   McFarland, L. V.; Mulligan, M. E.; Kwok, R. Y.; Stamm, W. E. Nosocomial acquisition of Clostridium difficile infection. *New England journal of medicine* **1989**, *320*, 204-210.

1215   (9)   Bartlett, J. G.; Perl, T. M. The new Clostridium difficile--what does it mean? *New*
1216   *England Journal of Medicine* **2005**, *353*, 2503-2504.
1217   (10)   Ozaki, E.; Kato, H.; Kita, H.; Karasawa, T.; Maegawa, T.; Koino, Y.; Matsumoto, K.;
1218   Takada, T.; Nomoto, K.; Tanaka, R. Clostridium difficile colonization in healthy adults: transient
1219   colonization and correlation with enterococcal colonization. *Journal of medical microbiology*
1220   **2004**, *53*, 167-172.
1221   (11)   Crobach, M. J.; Vernon, J. J.; Loo, V. G.; Kong, L. Y.; Péchiné, S.; Wilcox, M. H.;
1222   Kuijper, E. J. Understanding Clostridium difficile colonization. *Clinical microbiology reviews*
1223   **2018**, *31*, 10.1128/cmr. 00021-00017.
1224   (12)   VanInsberghe, D.; Elsherbini, J. A.; Varian, B.; Poutahidis, T.; Erdman, S.; Polz, M. F.
1225   Diarrhoeal events can trigger long-term Clostridium difficile colonization with recurrent blooms.
1226   *Nature microbiology* **2020**, *5*, 642-650.
1227   (13)   Hromada, S.; Venturelli, O. S. Gut microbiota interspecies interactions shape the
1228   response of Clostridioides difficile to clinically relevant antibiotics. *Plos Biology* **2023**, *21*,
1229   e3002100.
1230   (14)   Hromada, S.; Qian, Y.; Jacobson, T. B.; Clark, R. L.; Watson, L.; Safdar, N.; Amador‐
1231   Noguez, D.; Venturelli, O. S. Negative interactions determine Clostridioides difficile growth in
1232   synthetic human gut communities. *Molecular systems biology* **2021**, *17*, e10355.
1233   (15)   Schaeffler, H.; Breitrueck, A. Clostridium difficile–from colonization to infection. *Frontiers*
1234   *in microbiology* **2018**, *9*, 332266.
1235   (16)   Zacharioudakis, I. M.; Zervou, F. N.; Pliakos, E. E.; Ziakas, P. D.; Mylonakis, E.
1236   Colonization with toxinogenic C. difficile upon hospital admission, and risk of infection: a
1237   systematic review and meta-analysis. *Official journal of the American College of*
1238   *Gastroenterology| ACG* **2015**, *110*, 381-390.
1239   (17)   Miles-Jay, A.; Snitkin, E. S.; Lin, M. Y.; Shimasaki, T.; Schoeny, M.; Fukuda, C.;
1240   Dangana, T.; Moore, N.; Sansom, S. E.; Yelin, R. D. Longitudinal genomic surveillance of
1241   carriage and transmission of Clostridioides difficile in an intensive care unit. *Nature Medicine*
1242   **2023**, *29*, 2526-2534.
1243   (18)   Fu, Y.; Luo, Y.; Grinspan, A. M. Epidemiology of community-acquired and recurrent
1244   Clostridioides difficile infection. *Therapeutic advances in gastroenterology* **2021**, *14*,
1245   17562848211016248.
1246   (19)   Riggs, M. M.; Sethi, A. K.; Zabarsky, T. F.; Eckstein, E. C.; Jump, R. L.; Donskey, C. J.
1247   Asymptomatic carriers are a potential source for transmission of epidemic and nonepidemic
1248   Clostridium difficile strains among long-term care facility residents. *Clinical infectious diseases*
1249   **2007**, *45*, 992-998.
1250   (20)   Curry, S. R.; Muto, C. A.; Schlackman, J. L.; Pasculle, A. W.; Shutt, K. A.; Marsh, J. W.;
1251   Harrison, L. H. Use of multilocus variable number of tandem repeats analysis genotyping to
1252   determine the role of asymptomatic carriers in Clostridium difficile transmission. *Clinical*
1253   *infectious diseases* **2013**, *57*, 1094-1102.
1254   (21)   Eyre, D. W.; Griffiths, D.; Vaughan, A.; Golubchik, T.; Acharya, M.; O'Connor, L.; Crook,
1255   D. W.; Walker, A. S.; Peto, T. E. Asymptomatic Clostridium difficile colonisation and onward
1256   transmission. *PloS one* **2013**, *8*, e78445.
1257   (22)   Shim, J. K.; Johnson, S.; Samore, M. H.; Bliss, D. Z.; Gerding, D. N. Primary
1258   symptomless colonisation by Clostridium difficile and decreased risk of subsequent diarrhoea.
1259   *The Lancet* **1998**, *351*, 633-636.
1260   (23)   Kyne, L.; Warny, M.; Qamar, A.; Kelly, C. P. Asymptomatic carriage of Clostridium
1261   difficile and serum levels of IgG antibody against toxin A. *New England Journal of Medicine*
1262   **2000**, *342*, 390-397.
1263   (24)   Kyne, L.; Warny, M.; Qamar, A.; Kelly, C. P. Association between antibody response to
1264   toxin A and protection against recurrent Clostridium difficile diarrhoea. *The Lancet* **2001**, *357*,
1265   189-193.

1266   (25)   Vincent, C.; Miller, M. A.; Edens, T. J.; Mehrotra, S.; Dewar, K.; Manges, A. R. Bloom
1267   and bust: intestinal microbiota dynamics in response to hospital exposures and Clostridium
1268   difficile colonization or infection. *Microbiome* **2016**, *4*, 1-11.
1269   (26)   Sambol, S. P.; Merrigan, M. M.; Tang, J. K.; Johnson, S.; Gerding, D. N. Colonization for
1270   the prevention of Clostridium difficile disease in hamsters. *The Journal of infectious diseases*
1271   **2002**, *186*, 1781-1789.
1272   (27)   Merrigan, M. M.; Sambol, S. P.; Johnson, S.; Gerding, D. N. Prevention of fatal
1273   Clostridium difficile–associated disease during continuous administration of clindamycin in
1274   hamsters. *The Journal of infectious diseases* **2003**, *188*, 1922-1927.
1275   (28)   Merrigan, M. M.; Sambol, S. P.; Johnson, S.; Gerding, D. N. New approach to the
1276   management of Clostridium difficile infection: colonisation with non-toxigenic C. difficile during
1277   daily ampicillin or ceftriaxone administration. *International journal of antimicrobial agents* **2009**,
1278   *33*, S46-S50.
1279   (29)   Collins, J.; Danhof, H.; Britton, R. A. The role of trehalose in the global spread of
1280   epidemic Clostridium difficile. *Gut Microbes* **2019**, *10*, 204-209.
1281   (30)   Knight, D. R.; Elliott, B.; Chang, B. J.; Perkins, T. T.; Riley, T. V. Diversity and evolution
1282   in the genome of Clostridium difficile. *Clinical microbiology reviews* **2015**, *28*, 721-741.
1283   (31)   He, M.; Sebaihia, M.; Lawley, T. D.; Stabler, R. A.; Dawson, L. F.; Martin, M. J.; Holt, K.
1284   E.; Seth-Smith, H. M.; Quail, M. A.; Rance, R. Evolutionary dynamics of Clostridium difficile over
1285   short and long time scales. *Proceedings of the National Academy of Sciences* **2010**, *107*, 7527-
1286   7532.
1287   (32)   Collins, J.; Robinson, C.; Danhof, H.; Knetsch, C.; Van Leeuwen, H.; Lawley, T.;
1288   Auchtung, J.; Britton, e. R. Dietary trehalose enhances virulence of epidemic Clostridium
1289   difficile. *Nature* **2018**, *553*, 291-294.
1290   (33)   Pearl Mizrahi, S.; Goyal, A.; Gore, J. Community interactions drive the evolution of
1291   antibiotic tolerance in bacteria. *Proceedings of the National Academy of Sciences* **2023**, *120*,
1292   e2209043119.
1293   (34)   Konstantinidis, D.; Pereira, F.; Geissen, E. M.; Grkovska, K.; Kafkia, E.; Jouhten, P.;
1294   Kim, Y.; Devendran, S.; Zimmermann, M.; Patil, K. R. Adaptive laboratory evolution of microbial
1295   co‐cultures for improved metabolite secretion. *Molecular systems biology* **2021**, *17*, e10189.
1296   (35)   Scheuerl, T.; Hopkins, M.; Nowell, R. W.; Rivett, D. W.; Barraclough, T. G.; Bell, T.
1297   Bacterial adaptation is constrained in complex communities. *Nature Communications* **2020**, *11*,
1298   754.
1299   (36)   Lawrence, D.; Fiegna, F.; Behrends, V.; Bundy, J. G.; Phillimore, A. B.; Bell, T.;
1300   Barraclough, T. G. Species interactions alter evolutionary responses to a novel environment.
1301   *PLoS biology* **2012**, *10*, e1001330.
1302   (37)   Fiegna, F.; Moreno-Letelier, A.; Bell, T.; Barraclough, T. G. Evolution of species
1303   interactions determines microbial community productivity in new environments. *The ISME*
1304   *journal* **2015**, *9*, 1235-1245.
1305   (38)   Barber, J. N.; Sezmis, A. L.; Woods, L. C.; Anderson, T. D.; Voss, J. M.; McDonald, M. J.
1306   The evolution of coexistence from competition in experimental co-cultures of Escherichia coli
1307   and Saccharomyces cerevisiae. *The ISME Journal* **2021**, *15*, 746-761.
1308   (39)   Barber, J. N.; Nicholson, L. C.; Woods, L. C.; Judd, L. M.; Sezmis, A. L.; Hawkey, J.;
1309   Holt, K. E.; McDonald, M. J. Species interactions constrain adaptation and preserve ecological
1310   stability in an experimental microbial community. *The ISME Journal* **2022**, *16*, 1442-1452.
1311   (40)   Friedman, J.; Higgins, L. M.; Gore, J. Community structure follows simple assembly
1312   rules in microbial microcosms. *Nature ecology & evolution* **2017**, *1*, 0109.
1313   (41)   Celiker, H.; Gore, J. Clustering in community structure across replicate ecosystems
1314   following a long-term bacterial evolution experiment. *Nature communications* **2014**, *5*, 4643.

1315 (42)   Meroz, N.; Tovi, N.; Sorokin, Y.; Friedman, J. Community composition of microbial
1316 microcosms follows simple assembly rules at evolutionary timescales. *Nature communications*
1317 **2021**, *12*, 1-9.
1318 (43)   Rosenzweig, R. F.; Sharp, R.; Treves, D. S.; Adams, J. Microbial evolution in a simple
1319 unstructured environment: genetic differentiation in Escherichia coli. *Genetics* **1994**, *137*, 903-
1320 917.
1321 (44)   Helling, R. B.; Vargas, C. N.; Adams, J. Evolution of Escherichia coli during growth in a
1322 constant environment. *Genetics* **1987**, *116*, 349-358.
1323 (45)   Johansson, J. Evolutionary responses to environmental changes: how does competition
1324 affect adaptation? *Evolution* **2008**, *62*, 421-435.
1325 (46)   Scheuerl, T.; Hopkins, M.; Nowell, R. W.; Rivett, D. W.; Barraclough, T. G.; Bell, T.
1326 Bacterial adaptation is constrained in complex communities. *Nature Communications* **2020**, *11*,
1327 1-8.
1328 (47)   Harcombe, W. Novel cooperation experimentally evolved between species. *Evolution*
1329 **2010**, *64*, 2166-2172.
1330 (48)   Harcombe, W. R.; Chacón, J. M.; Adamowicz, E. M.; Chubiz, L. M.; Marx, C. J. Evolution
1331 of bidirectional costly mutualism from byproduct consumption. *Proceedings of the National*
1332 *Academy of Sciences* **2018**, *115*, 12000-12004.
1333 (49)   Turkarslan, S.; Stopnisek, N.; Thompson, A. W.; Arens, C. E.; Valenzuela, J. J.; Wilson,
1334 J.; Hunt, K. A.; Hardwicke, J.; de Lomana, A. L. G.; Lim, S. Synergistic epistasis enhances the
1335 co-operativity of mutualistic interspecies interactions. *The ISME Journal* **2021**, *15*, 2233-2247.
1336 (50)   Hansen, S. K.; Rainey, P. B.; Haagensen, J. A.; Molin, S. Evolution of species
1337 interactions in a biofilm community. *Nature* **2007**, *445*, 533-536.
1338 (51)   Clark, R. L.; Connors, B. M.; Stevenson, D. M.; Hromada, S. E.; Hamilton, J. J.; Amador-
1339 Noguez, D.; Venturelli, O. S. Design of synthetic human gut microbiome assembly and butyrate
1340 production. *Nature communications* **2021**, *12*, 1-16.
1341 (52)   Ostrem Loss, E.; Thompson, J.; Cheung, P. L. K.; Qian, Y.; Venturelli, O. S.
1342 Carbohydrate complexity limits microbial growth and reduces the sensitivity of human gut
1343 communities to perturbations. *Nature ecology & evolution* **2023**, *7*, 127-142.
1344 (53)   Forster, S. C.; Kumar, N.; Anonye, B. O.; Almeida, A.; Viciani, E.; Stares, M. D.; Dunn,
1345 M.; Mkandawire, T. T.; Zhu, A.; Shao, Y. A human gut bacterial genome and culture collection
1346 for improved metagenomic analyses. *Nature biotechnology* **2019**, *37*, 186-192.
1347 (54)   Buffie, C. G.; Bucci, V.; Stein, R. R.; McKenney, P. T.; Ling, L.; Gobourne, A.; No, D.;
1348 Liu, H.; Kinnebrew, M.; Viale, A. Precision microbiome reconstitution restores bile acid mediated
1349 resistance to Clostridium difficile. *Nature* **2015**, *517*, 205-208.
1350 (55)   Sulaiman, J. E.; Thompson, J.; Qian, Y.; Vivas, E. I.; Diener, C.; Gibbons, S.; Safdar, N.;
1351 Venturelli, O. S. Elucidating human gut microbiota interactions that robustly inhibit diverse
1352 *Clostridioides difficile* strains across different nutrient landscapes. *BioRxiv* **2024**.
1353 (56)   Ferreyra, J. A.; Wu, K. J.; Hryckowian, A. J.; Bouley, D. M.; Weimer, B. C.; Sonnenburg,
1354 J. L. Gut microbiota-produced succinate promotes C. difficile infection after antibiotic treatment
1355 or motility disturbance. *Cell host & microbe* **2014**, *16*, 770-777.
1356 (57)   Ghimire, S.; Roy, C.; Wongkuna, S.; Antony, L.; Maji, A.; Keena, M. C.; Foley, A.; Scaria,
1357 J. Identification of Clostridioides difficile-inhibiting gut commensals using culturomics,
1358 phenotyping, and combinatorial community assembly. *Msystems* **2020**, *5*, 10.1128/msystems.
1359 00620-00619.
1360 (58)   Pereira, F. C.; Wasmund, K.; Cobankovic, I.; Jehmlich, N.; Herbold, C. W.; Lee, K. S.;
1361 Sziranyi, B.; Vesely, C.; Decker, T.; Stocker, R. Rational design of a microbial consortium of
1362 mucosal sugar utilizers reduces Clostridiodes difficile colonization. *Nature communications*
1363 **2020**, *11*, 1-15.

(59)   Hassall, J.; Cheng, J. K.; Unnikrishnan, M. Dissecting individual interactions between pathogenic and commensal bacteria within a multispecies gut microbial community. *Msphere* **2021**, *6*, 10.1128/msphere. 00013-00021.

(60)   Venturelli, O. S.; Carr, A. V.; Fisher, G.; Hsu, R. H.; Lau, R.; Bowen, B. P.; Hromada, S.; Northen, T.; Arkin, A. P. Deciphering microbial interactions in synthetic human gut microbiome communities. *Molecular systems biology* **2018**, *14*, e8157.

(61)   Connors, B. M.; Thompson, J.; Ertmer, S.; Clark, R. L.; Pfleger, B. F.; Venturelli, O. S. Control points for design of taxonomic composition in synthetic human gut communities. *Cell Systems* **2023**, *14*, 1044-1058. e1013.

(62)   Coyte, K. Z.; Schluter, J.; Foster, K. R. The ecology of the microbiome: networks, competition, and stability. *Science* **2015**, *350*, 663-666.

(63)   Patel, S.; Cortez, M. H.; Schreiber, S. J. Partitioning the effects of eco-evolutionary feedbacks on community stability. *The American Naturalist* **2018**, *191*, 381-394.

(64)   Alon, U.: *An introduction to systems biology: design principles of biological circuits*; Chapman and Hall/CRC, 2019.

(65)   Aguirre, A. M.; Yalcinkaya, N.; Wu, Q.; Swennes, A.; Tessier, M. E.; Roberts, P.; Miyajima, F.; Savidge, T.; Sorg, J. A. Bile acid-independent protection against Clostridioides difficile infection. *PLoS Pathogens* **2021**, *17*, e1010015.

(66)   Kang, J. D.; Myers, C. J.; Harris, S. C.; Kakiyama, G.; Lee, I.-K.; Yun, B.-S.; Matsuzaki, K.; Furukawa, M.; Min, H.-K.; Bajaj, J. S. Bile acid 7α-dehydroxylating gut bacteria secrete antibiotics that inhibit Clostridium difficile: role of secondary bile acids. *Cell chemical biology* **2019**, *26*, 27-34. e24.

(67)   Ridlon, J. M.; Kang, D.-J.; Hylemon, P. B. Bile salt biotransformations by human intestinal bacteria. *Journal of lipid research* **2006**, *47*, 241-259.

(68)   Ridlon, J. M.; Harris, S. C.; Bhowmik, S.; Kang, D.-J.; Hylemon, P. B. Consequences of bile salt biotransformations by intestinal bacteria. *Gut microbes* **2016**, *7*, 22-39.

(69)   Ridlon, J. M.; Devendran, S.; Alves, J. M.; Doden, H.; Wolf, P. G.; Pereira, G. V.; Ly, L.; Volland, A.; Takei, H.; Nittono, H. The 'in vivo lifestyle' of bile acid 7α-dehydroxylating bacteria: comparative genomics, metatranscriptomic, and bile acid metabolomics analysis of a defined microbial community in gnotobiotic mice. *Gut microbes* **2020**, *11*, 381-404.

(70)   Scaria, J.; Ponnala, L.; Janvilisri, T.; Yan, W.; Mueller, L. A.; Chang, Y.-F. Analysis of ultra low genome conservation in Clostridium difficile. *PLoS one* **2010**, *5*, e15147.

(71)   Janvilisri, T.; Scaria, J.; Thompson, A. D.; Nicholson, A.; Limbago, B. M.; Arroyo, L. G.; Songer, J. G.; Gröhn, Y. T.; Chang, Y.-F. Microarray identification of Clostridium difficile core components and divergent regions associated with host origin. *Journal of Bacteriology* **2009**, *191*, 3881-3891.

(72)   Stubbs, S. L.; Brazier, J. S.; O'Neill, G. L.; Duerden, B. I. PCR targeted to the 16S-23S rRNA gene intergenic spacer region of Clostridium difficile and construction of a library consisting of 116 different PCR ribotypes. *Journal of clinical microbiology* **1999**, *37*, 461-463.

(73)   Knight, D. R.; Imwattana, K.; Kullin, B.; Guerrero-Araya, E.; Paredes-Sabja, D.; Didelot, X.; Dingle, K. E.; Eyre, D. W.; Rodríguez, C.; Riley, T. V. Major genetic discontinuity and novel toxigenic species in Clostridioides difficile taxonomy. *Elife* **2021**, *10*, e64325.

(74)   Neumann-Schaal, M.; Jahn, D.; Schmidt-Hohagen, K. Metabolism the difficile way: the key to the success of the pathogen Clostridioides difficile. *Frontiers in microbiology* **2019**, *10*, 219.

(75)   Sears, C. L. A dynamic partnership: celebrating our gut flora. *Anaerobe* **2005**, *11*, 247-251.

(76)   Almeida, A.; Mitchell, A. L.; Boland, M.; Forster, S. C.; Gloor, G. B.; Tarkowska, A.; Lawley, T. D.; Finn, R. D. A new genomic blueprint of the human gut microbiota. *Nature* **2019**, *568*, 499-504.

(77)   Qin, J.; Li, R.; Raes, J.; Arumugam, M.; Burgdorf, K. S.; Manichanh, C.; Nielsen, T.; Pons, N.; Levenez, F.; Yamada, T. A human gut microbial gene catalogue established by metagenomic sequencing. *nature* **2010**, *464*, 59-65.

(78)   Feng, J.; Qian, Y.; Zhou, Z.; Ertmer, S.; Vivas, E. I.; Lan, F.; Hamilton, J. J.; Rey, F. E.; Anantharaman, K.; Venturelli, O. S. Polysaccharide utilization loci in Bacteroides determine population fitness and community-level interactions. *Cell host & microbe* **2022**, *30*, 200-215. e212.

(79)   Bouillaut, L.; Self, W. T.; Sonenshein, A. L. Proline-dependent regulation of Clostridium difficile Stickland metabolism. *Journal of bacteriology* **2013**, *195*, 844-854.

(80)   Battaglioli, E. J.; Hale, V. L.; Chen, J.; Jeraldo, P.; Ruiz-Mojica, C.; Schmidt, B. A.; Rekdal, V. M.; Till, L. M.; Huq, L.; Smits, S. A. Clostridioides difficile uses amino acids associated with gut microbial dysbiosis in a subset of patients with diarrhea. *Science translational medicine* **2018**, *10*, eaam7019.

(81)   Han, S.; Van Treuren, W.; Fischer, C. R.; Merrill, B. D.; DeFelice, B. C.; Sanchez, J. M.; Higginbottom, S. K.; Guthrie, L.; Fall, L. A.; Dodd, D. A metabolomics pipeline for the mechanistic interrogation of the gut microbiome. *Nature* **2021**, *595*, 415-420.

(82)   Medlock, G. L.; Carey, M. A.; McDuffie, D. G.; Mundy, M. B.; Giallourou, N.; Swann, J. R.; Kolling, G. L.; Papin, J. A. Inferring metabolic mechanisms of interaction within a defined gut microbiota. *Cell systems* **2018**, *7*, 245-257. e247.

(83)   Catlett, J. L.; Catazaro, J.; Cashman, M.; Carr, S.; Powers, R.; Cohen, M. B.; Buan, N. R. Metabolic feedback inhibition influences metabolite secretion by the human gut symbiont Bacteroides thetaiotaomicron. *Msystems* **2020**, *5*, 10.1128/msystems. 00252-00220.

(84)   Reed, A.; Nethery, M.; Stewart, A.; Barrangou, R.; Theriot, C. Strain-dependent inhibition of Clostridioides difficile by commensal Clostridia carrying the bile acid-inducible (bai) operon. *Journal of bacteriology* **2020**, *202*, 10.1128/jb. 00039-00020.

(85)   Brochet, S.; Quinn, A.; Mars, R. A.; Neuschwander, N.; Sauer, U.; Engel, P. Niche partitioning facilitates coexistence of closely related honey bee gut bacteria. *elife* **2021**, *10*, e68583.

(86)   Fischbach, M. A.; Sonnenburg, J. L. Eating for two: how metabolism establishes interspecies interactions in the gut. *Cell host & microbe* **2011**, *10*, 336-347.

(87)   Zhao, S.; Lieberman, T. D.; Poyet, M.; Kauffman, K. M.; Gibbons, S. M.; Groussin, M.; Xavier, R. J.; Alm, E. J. Adaptive evolution within gut microbiomes of healthy people. *Cell host & microbe* **2019**, *25*, 656-667. e658.

(88)   Rivière, A.; Selak, M.; Lantin, D.; Leroy, F.; De Vuyst, L. Bifidobacteria and butyrate-producing colon bacteria: importance and strategies for their stimulation in the human gut. *Frontiers in microbiology* **2016**, *7*, 979.

(89)   Fachi, J. L.; de Souza Felipe, J.; Pral, L. P.; da Silva, B. K.; Corrêa, R. O.; de Andrade, M. C. P.; da Fonseca, D. M.; Basso, P. J.; Câmara, N. O. S.; e Souza, É. L. d. S. Butyrate protects mice from Clostridium difficile-induced colitis through an HIF-1-dependent mechanism. *Cell reports* **2019**, *27*, 750-761. e757.

(90)   Park, S.-Y.; Rao, C.; Coyte, K. Z.; Kuziel, G. A.; Zhang, Y.; Huang, W.; Franzosa, E. A.; Weng, J.-K.; Huttenhower, C.; Rakoff-Nahoum, S. Strain-level fitness in the gut microbiome is an emergent property of glycans and a single metabolite. *Cell* **2022**, *185*, 513-529. e521.

(91)   Baranwal, M.; Clark, R. L.; Thompson, J.; Sun, Z.; Hero, A. O.; Venturelli, O. S. Recurrent neural networks enable design of multifunctional synthetic human gut microbiome dynamics. *Elife* **2022**, *11*, e73870.

(92)   Bouillaut, L.; Dubois, T.; Sonenshein, A. L.; Dupuy, B. Integration of metabolism and virulence in Clostridium difficile. *Research in microbiology* **2015**, *166*, 375-383.

(93)   Neumann-Schaal, M.; Hofmann, J. D.; Will, S. E.; Schomburg, D. Time-resolved amino acid uptake of Clostridium difficile 630Δerm and concomitant fermentation product and toxin formation. *BMC microbiology* **2015**, *15*, 1-12.

(94)   Yamakawa, K.; Kamiya, S.; Meng, X.; Karasawa, T.; Nakamura, S. Toxin production by Clostridium difficile in a defined medium with limited amino acids. *Journal of medical microbiology* **1994**, *41*, 319-323.

(95)   Jenior, M. L.; Leslie, J. L.; Young, V. B.; Schloss, P. D. Clostridium difficile colonizes alternative nutrient niches during infection across distinct murine gut microbiomes. *MSystems* **2017**, *2*, 10.1128/msystems. 00063-00017.

(96)   Round, J. L.; Mazmanian, S. K. The gut microbiota shapes intestinal immune responses during health and disease. *Nature reviews immunology* **2009**, *9*, 313-323.

(97)   Ghimire, S.; Roy, C.; Wongkuna, S.; Antony, L.; Maji, A.; Keena, M. C.; Foley, A.; Scaria, J. Identification of Clostridioides difficile-inhibiting gut commensals using culturomics, phenotyping, and combinatorial community assembly. *Msystems* **2020**, *5*, e00620-00619.

(98)   Theriot, C. M.; Koenigsknecht, M. J.; Carlson, P. E.; Hatton, G. E.; Nelson, A. M.; Li, B.; Huffnagle, G. B.; Z Li, J.; Young, V. B. Antibiotic-induced shifts in the mouse gut microbiome and metabolome increase susceptibility to Clostridium difficile infection. *Nature communications* **2014**, *5*, 1-10.

(99)   Kelly, C. R.; Khoruts, A.; Staley, C.; Sadowsky, M. J.; Abd, M.; Alani, M.; Bakow, B.; Curran, P.; McKenney, J.; Tisch, A. Effect of fecal microbiota transplantation on recurrence in multiply recurrent Clostridium difficile infection: a randomized trial. *Annals of internal medicine* **2016**, *165*, 609-616.

(100)   Reveles, K. R.; Lee, G. C.; Boyd, N. K.; Frei, C. R. The rise in Clostridium difficile infection incidence among hospitalized adults in the United States: 2001-2010. *American journal of infection control* **2014**, *42*, 1028-1032.

(101)   Evans, C. T.; Safdar, N. Current trends in the epidemiology and outcomes of Clostridium difficile infection. *Clinical Infectious Diseases* **2015**, *60*, S66-S71.

(102)   Barbut, F.; Jones, G.; Eckert, C. Epidemiology and control of Clostridium difficile infections in healthcare settings: an update. *Current opinion in infectious diseases* **2011**, *24*, 370-376.

(103)   Hu, J.; Amor, D. R.; Barbier, M.; Bunin, G.; Gore, J. Emergent phases of ecological diversity and dynamics mapped in microcosms. *Science* **2022**, *378*, 85-89.

(104)   Ratzke, C.; Barrere, J.; Gore, J. Strength of species interactions determines biodiversity and stability in microbial communities. *Nature ecology & evolution* **2020**, *4*, 376-383.

(105)   Ratzke, C.; Gore, J. Modifying and reacting to the environmental pH can drive bacterial interactions. *PLoS biology* **2018**, *16*, e2004248.

(106)   Smillie, C. S.; Sauk, J.; Gevers, D.; Friedman, J.; Sung, J.; Youngster, I.; Hohmann, E. L.; Staley, C.; Khoruts, A.; Sadowsky, M. J. Strain tracking reveals the determinants of bacterial engraftment in the human gut following fecal microbiota transplantation. *Cell host & microbe* **2018**, *23*, 229-240. e225.

(107)   Kumar, R.; Yi, N.; Zhi, D.; Eipers, P.; Goldsmith, K. T.; Dixon, P.; Crossman, D. K.; Crowley, M. R.; Lefkowitz, E. J.; Rodriguez, J. M. Identification of donor microbe species that colonize and persist long term in the recipient after fecal transplant for recurrent Clostridium difficile. *NPJ biofilms and microbiomes* **2017**, *3*, 12.

(108)   Aggarwala, V.; Mogno, I.; Li, Z.; Yang, C.; Britton, G. J.; Chen-Liaw, A.; Mitcham, J.; Bongers, G.; Gevers, D.; Clemente, J. C. Precise quantification of bacterial strains after fecal microbiota transplantation delineates long-term engraftment and explains outcomes. *Nature Microbiology* **2021**, *6*, 1309-1318.

(109)   Goyal, A.; Wang, T.; Dubinkina, V.; Maslov, S. Ecology-guided prediction of cross-feeding interactions in the human gut microbiome. *Nature communications* **2021**, *12*, 1335.

(110)   Kumar, N.; Browne, H. P.; Viciani, E.; Forster, S. C.; Clare, S.; Harcourt, K.; Stares, M. D.; Dougan, G.; Fairley, D. J.; Roberts, P. Adaptation of host transmission cycle during Clostridium difficile speciation. *Nature genetics* **2019**, *51*, 1315-1320.

(111) Kulecka, M.; Waker, E.; Ambrozkiewicz, F.; Paziewska, A.; Skubisz, K.; Cybula, P.; Targoński, Ł.; Mikula, M.; Walewski, J.; Ostrowski, J. Higher genome variability within metabolism genes associates with recurrent Clostridium difficile infection. *BMC microbiology* **2021**, *21*, 1-10.

(112) Stabler, R. A.; He, M.; Dawson, L.; Martin, M.; Valiente, E.; Corton, C.; Lawley, T. D.; Sebaihia, M.; Quail, M. A.; Rose, G. Comparative genome and phenotypic analysis of Clostridium difficile 027 strains provides insight into the evolution of a hypervirulent bacterium. *Genome biology* **2009**, *10*, 1-15.

(113) Norsigian, C. J.; Danhof, H. A.; Brand, C. K.; Oezguen, N.; Midani, F. S.; Palsson, B. O.; Savidge, T. C.; Britton, R. A.; Spinler, J. K.; Monk, J. M. Systems biology analysis of the Clostridioides difficile core-genome contextualizes microenvironmental evolutionary pressures leading to genotypic and phenotypic divergence. *NPJ systems biology and applications* **2020**, *6*, 1-12.

(114) Dong, Q.; Lin, H.; Allen, M.-M.; Garneau, J. R.; Sia, J. K.; Smith, R. C.; Haro, F.; McMillen, T.; Pope, R. L.; Metcalfe, C. Virulence and genomic diversity among clinical isolates of ST1 (BI/NAP1/027) Clostridioides difficile. *Cell reports* **2023**, *42*.

(115) Dong, Q.; Harper, S.; McSpadden, E.; Son, S.; Allen, M.-M.; Lin, H.; Smith, R.; Metcalfe, C.; Burgo, V.; Woodson, C.; Sundararajan, A.; Rose, A.; McMillin, M.; Moran, D.; Little, J.; Mullowney, M.; Sidebottom, A.; Shen, A.; Fortier, L.-C.; Pamer, E. Protection against Clostridioides difficile disease by a naturally avirulent C. difficile strain. *BioRxiv* **2024**.

(116) Lenski, R. E.; Travisano, M. Dynamics of adaptation and diversification: a 10,000-generation experiment with bacterial populations. *Proceedings of the National Academy of Sciences* **1994**, *91*, 6808-6814.

(117) Zhang, J.; Kobert, K.; Flouri, T.; Stamatakis, A. PEAR: a fast and accurate Illumina Paired-End reAd mergeR. *Bioinformatics* **2014**, *30*, 614-620.

(118) Wang, Q.; Garrity, G. M.; Tiedje, J. M.; Cole, J. R. Naive Bayesian classifier for rapid assignment of rRNA sequences into the new bacterial taxonomy. *Applied and environmental microbiology* **2007**, *73*, 5261-5267.

(119) Schloss, P. D.; Westcott, S. L.; Ryabin, T.; Hall, J. R.; Hartmann, M.; Hollister, E. B.; Lesniewski, R. A.; Oakley, B. B.; Parks, D. H.; Robinson, C. J. Introducing mothur: open-source, platform-independent, community-supported software for describing and comparing microbial communities. *Applied and environmental microbiology* **2009**, *75*, 7537-7541.

(120) Bishop, C.: Pattern Recognition and Machine Learning Chris Bishop. Springer: Berlin/Heidelberg, Germany, 2004.

(121) Rowan, T. H.: *Functional stability analysis of numerical algorithms*; The University of Texas at Austin, 1990.

(122) Johnson, S. G.: The NLopt nonlinear-optimization package. 2014.

(123) Kucherenko, S.; Sytsko, Y. Application of deterministic low-discrepancy sequences in global optimization. *Computational Optimization and Applications* **2005**, *30*, 297-318.

(124) Rinnooy Kan, A.; Timmer, G. T. Stochastic global optimization methods part I: Clustering methods. *Mathematical programming* **1987**, *39*, 27-56.

(125) Deatherage, D. E.; Barrick, J. E. Identification of mutations in laboratory-evolved microbes from next-generation sequencing data using breseq. *Engineering and analyzing multicellular systems: methods and protocols* **2014**, 165-188.

(126) Seemann, T.: Snippy: fast bacterial variant calling from NGS reads. 2015.

(127) Andrews, S.: FastQC: a quality control tool for high throughput sequence data. Babraham Bioinformatics, Babraham Institute, Cambridge, United Kingdom, 2010.

(128) Bushnell, B. *BBMap: a fast, accurate, splice-aware aligner*2014.

(129) Liao, Y.; Smyth, G. K.; Shi, W. featureCounts: an efficient general purpose program for assigning sequence reads to genomic features. *Bioinformatics* **2014**, *30*, 923-930.

1565   (130)   Love, M. I.; Huber, W.; Anders, S. Moderated estimation of fold change and dispersion
1566   for RNA-seq data with DESeq2. *Genome biology* **2014**, *15*, 1-21.
1567   (131)   Zhu, A.; Ibrahim, J. G.; Love, M. I. Heavy-tailed prior distributions for sequence count
1568   data: removing the noise and preserving large differences. *Bioinformatics* **2019**, *35*, 2084-2092.
1569   (132)   Goodman, A. L.; Kallstrom, G.; Faith, J. J.; Reyes, A.; Moore, A.; Dantas, G.; Gordon, J.
1570   I. Extensive personal human gut microbiota culture collections characterized and manipulated in
1571   gnotobiotic mice. *Proceedings of the National Academy of Sciences* **2011**, *108*, 6252-6257.

1572